Elsevier Editorial System(tm) for Materials Science & Engineering A
Manuscript Draft

Manuscript Number: MSEA-D-19-00184R1

Title: Conventional and cooling assisted friction stir welding of AA6061 and AZ31B alloys

Article Type: Research Paper

Keywords: cooling assisted friction stir welding; dissimilar joint; mechanical properties; microstructure; intermetallic compounds

Corresponding Author: Dr. Antonello Astarita, Ph.D.

Corresponding Author's Institution: University of Naples

First Author: Kush P Mehta, Ph.D.

Order of Authors: Kush P Mehta, Ph.D.; Pierpaolo Carlone, Ph.D.; Antonello Astarita, Ph.D.; Fabio Scherillo, Ph.D.; Felice Rubino, Ph.D.; Poojan J Vora, B.Tech

Abstract: Conventional and cooling assisted friction stir welded Al-Mg joints were investigated by visual inspection, optical macro plus microscopy, scanning electron micrographs, energy dispersive X-ray spectroscopy, X-ray diffractions, tensile testing and micro hardness indentation. The nugget zone is characterized by onion rings composed of different phases such as Mg in an Al matrix, Al in an Mg matrix as well as intermetallic compounds, Al3Mg2 and Al12Mg17. A diffusion layer was detected on the Al side of the joint between the nugget and thermo-mechanically affected zones identifying a solid solution of Mg in Al. No diffusion layer was observed on the Mg side. The tensile strength of the dissimilar joints is enhanced by cooling assisted welding process due to the reduction in the amount of intermetallic compounds inside the weld bead. Congruently, higher hardness peaks are reported in the nugget zone of conventional FSW joint with respect to the CFSW joint.

Prof. Antonello Astarita, PhD
Phone: 0039 081 7682364
E-mail: antonello.astarita@unina.it

January 9th, 2019

Prof E. J. Lavernia
Editor in Chief of the Journal of Material Science and Engineering: part A

Dear Professor Lavernia,

Please find enclosed our manuscript, "Conventional and cooling assisted friction stir welding of AA6061 and AZ31B alloys" by Kush P. Mehta, Pierpaolo Carlone, Antonello Astarita, Fabio Scherillo, Felice Rubino, Poojan Vora, which we would like to submit again for publication in the Journal of Material Science and Engineering: part A.

This manuscript discusses the dissimilar solid state joining by conventional friction stir welding and cooling assisted friction stir welding of AA6061 aluminum alloy to AZ31B magnesium alloy, demonstrating some advantages of the latter process with respect to joint soundness and mechanical properties. Within the manuscript, processing details, metallurgical aspect (absolutely intriguing in authors' personal opinion) investigated by optical microscopy, SEM and XRD analysis were reported and discussed.

Considering the significant challenges related to the welding of the indicated materials, as well as the commented outcomes, authors firmly believe that the presented methodologies and results are of interest for the academic and industrial communities active in the field of solid state (similar and dissimilar), mainly related to the aerospace and automotive sectors.

We confirm that this manuscript has not submitted for publication elsewhere. No other paper has been published or submitted using the same data set.

Taking into account the relevancy of the investigated topic and the effectiveness of the used techniques, we are confident that the paper would appeal to the readership of your journal. Looking forward to hear your and referees' comments,

Sincerely,

Antonello Astarita

Answer to the reviewers' comments

Dear Editor,

On behalf of all authors I would like to gratefully acknowledge you and the reviewers for carefully reading the paper and the thoughtful comments provided. The manuscript has been revised taking into account all referee's suggestions and editorial indications to prepare the revised manuscript and contributed to make the article clearer, more compelling, and broader.

All the changes have been highlighted in red in the revised manuscript. In the following the detailed answers to all the comments, below you can find the detailed answers to the reviewer comment.

Reviewer(s)' Comments to Author:

1. The introduction part is too wordy on the other variations of conventional assisted friction stir welding and does not highlight the novelty of the current research well.

Thanks for this suggestion; the introduction has been revised accordingly. In particular some lines of text regarding the other variations of the process have been removed (erased in "revision format" within the revised manuscript) and a paragraph has been added to better highlight the novelty of the current research.

2. The link between the dramatical enhancement of tensile strength and the microstructure is not fully elucidated. Though the authors state that "Mofid et al. (2012b) mentioned that brittle form of IMCs is a major reason for the crack, because the fracture preferentially propagated along the brittle intermetallic layers, as confirmed by the cleavage-type fracture surfaces observed", showing the stress-strain curves, optical macro plus microscopy and/or scanning electron micrographs of the fracture surface of these two types of joints will be very helpful.

Optical images of the failed specimens as well as SEM micrographs of the fracture surfaces have been added and discussed within the manuscript.

3. There are many undefined terminologies in the manuscript, such as IMC, TIG. Please go through the manuscript carefully to fix these typos.

All the used acronyms were properly checked and the typos were fixed.

Conventional and cooling assisted friction stir welding of AA6061 and AZ31B alloys

Kush P Mehta[1], Pierpaolo Carlone[2], Antonello Astarita[3], Fabio Scherillo[3], Felice Rubino[2], Poojan Vora[1]

[1]Department of Mechanical Engineering, School of Technology (SOT), Pandit Deendayal Petroleum University (PDPU), Raisan, Gandhinagar 382007, Gujarat, India.

[2]Department of Industrial Engineering, University of Salerno, Via Giovanni Paolo II, 132, 84084, Fisciano (SA), Italy.

[3]Department of Chemical, Materials and Industrial Production Engineering, University of Naples, "Federico II", P.le Tecchio 80, 80100 Naples, Italy

Abstract

Conventional and cooling assisted friction stir welded Al-Mg joints were investigated by visual inspection, optical macro plus microscopy, scanning electron micrographs, energy dispersive X-ray spectroscopy, X-ray diffractions, tensile testing and micro hardness indentation. The nugget zone is characterized by onion rings composed of different phases such as Mg in an Al matrix, Al in an Mg matrix as well as intermetallic compounds, Al_3Mg_2 and $Al_{12}Mg_{17}$. A diffusion layer was detected on the Al side of the joint between the nugget and thermo-mechanically affected zones identifying a solid solution of Mg in Al. No diffusion layer was observed on the Mg side. The tensile strength of the dissimilar joints is enhanced by cooling assisted welding process due to the reduction in the amount of intermetallic compounds inside the weld bead. Congruently, higher hardness peaks are reported in the nugget zone of conventional FSW joint with respect to the CFSW joint.

Keywords: cooling assisted friction stir welding, dissimilar joint, mechanical properties, microstructure, intermetallic compounds

1. Introduction

Friction stir welding (FSW) is observed as qualified technique to obtain sound dissimilar joints adopting different pairs of metallic materials, such as Al-Cu, Al-Mg and Al-steel structures. Mehta and Badheka (2017) provided comprehensive investigation on joining of Aluminum (Al)-Copper (Cu) by means of FSW technology, pointing that, despite the potential benefits, the pronounced formation of intermetallic compounds due to the limited solubility of Al and Cu at room temperature lowers the quality of the joints. The authors concluded that novel variations in the conventional FSW were proved to be able to enhance the performances of the Al-Cu system. Shah et al. (2018) reviewed the bonding mechanisms of FS welded Al-Magnesium (Mg). The authors stated that the heat dissipated in the material during the process significantly affects the amount of intermetallic compounds (IMCs) from the welding process. In particular, process parameters such as base metal positioning, tool offset and revolutionary pitch (defined as ratio between and tool welding and rotational speeds) dictate the heat input, ruling the Al-Mg joint interface and the joint efficiency. Suppression of excessive heat showed to be a promising solution to limit the IMC growth and improve the overall joint quality. Shah and Ishak (2014) and Atabaki et al. (2014) pointed out the relevance of the welding parameters synergy to control type, size and amount of Fe/Al compounds. In particular, thick layers of different intermetallic (e.g. $FeAl_3$, Fe_2Al_5 and $FeAl_2$) observed at the faying surfaces depending on the rotational speed and pin depth adopted. Preheating of welding materials with FSW technique demonstrated to be suitable strategies to overcome the limitations of conventional processes. DebRoy and Bhadeshia (2010) and Simar and Avettand-Fènoël (2017) reviewed other different dissimilar materials structure, including Al-titanium (Ti), Ti-steel, Mg-steel, and Mg-Ti summarizing the guidelines to tune-up the process parameters in order to manufacture sound and free-defects welds. The main issues that have to be addressed during a dissimilar FSW are related to: i) the different plasticisation temperatures of the metals that affect the material flow and ii) the constitutional liquation that coupled with the reciprocal affinity of metals dictates the IMC nature and distribution. As far the material flow, the authors suggest to place the softer material on the retreating side (RS) and offset the tool toward the advancing side (AS), where the harder material should be placed, in order to increase the heat input and promote a vortex-like flow that enhances the joint properties. At the same time, more pronounced heat input favours the IMCs formation and increases the thickness of the IMCs layer, especially for Al-Cu, Al-Ti and Al-Mg pairs characterized by a low melting eutectic phase. A limited IMC layer, approximately in the range of 2 – 4 μm, is instead desirable to enhance the joint strength. Variations in the process conditions of conventional FSW are suggested to deal with competitive-nature phenomena involved in the welding and thus enhance the properties in dissimilar joints. Safi et al. (2016) argued that warm FSW (WFSW) provides improved mechanical properties of Al-Cu system. Yaduwanshi et al. (2016) experimented a plasma assisted FSW for dissimilar Al-Cu system and claimed an increase in joint efficiency. Liu et al. (2015) implemented electrically assisted FSW and tested it on dissimilar AA6061-TRIP steel 780 welding. Bang et al. (2012) obtained improved joint strength relative to Al base material with gas tungsten arc welding (GTAW) assisted FSW for dissimilar aluminum alloy-stainless steel pair.. Similar to aforementioned dissimilar systems, Al-Mg system have been also subjected to hybrid FSW as limitedly reported. Chang et al. (2011) improved tensile strength by introducing Ni foil third material with laser assisted FSW process variation due to the less formation of IMCs for AZ31B-H24 to AA6061-T6 system observed. Ji et al. (2017a) obtained relatively thicker IMC layer promoting the creation of the joint by having stationary shoulder diameter FSW for dissimilar AZ31B to AA6061 system. Ji et al. (2017b) and Lv et al. (2018) improved the AZ31B-AA6061 joint by ultrasonic assisted FSW. Further variations in the FSW process of stationary shoulder with ultrasonic assistance were developed by Liu et al. (2018) for AZ31B-AA6061 system, wherein noted improvements in formation of IMCs and tensile properties.

Apart from conventional FSW and process variations with heating enhanced FSW, the concept of cooling submerged FSW is rudimentary reported. Mehta and Badheka (2017) drastically reduced the formation of IMCs and enhanced tensile strength with water cooling assisted FSW in case of Al-Cu structure. In case of AZ31-AA5083 system, Mofid et al. (2012a) and Mofid et al. (2012b) suppressed the formation of IMCs with the effect of submerged FSW in underwater and under liquid nitrogen conditions respectively. Zhao et al. (2015) conducted similar concept of underwater FSW for AZ31-AA6013 system and found better tensile properties. In practice, it is very difficult to subject the workpiece to underwater or any other submerged cooling source, therefore, cooling assisted FSW (CFSW) process variation, where cooling nozzle is subjected behind FSW tool, is suggested in the present study. In this variant of the process, here applied for the first time in the dissimilar welding of aluminum to magnesium, the heating of the adjoining material is reduced due to applied cooling facility. Consequently, a relatively minor amount of IMCs is formed, leading to enhanced mechanical properties. If compared to the submerged FSW process, the CFSW process allows one to better control the heat removal from the material to be welded. Aiming to investigate the effectiveness of CFSW process, exclusive comparisons of microstructural features, IMCs formation and mechanical properties of friction stir welded Al-Mg joints obtained with and without cooling source are comprehensively presented in this investigation.

2. Materials and methods

6 mm thick AA6061 aluminum alloy and AZ31B magnesium alloy were used as base materials for dissimilar joining by FSW and CFSW in this study. Butt joint configuration was considered. Composition and properties of base materials are mentioned in Table 1 and Table 2, respectively. The used tool, in both welding processes, was realized in H13 material, with shoulder diameter of 20 mm, pin diameter of 7 mm and 1 mm pitch left hand threaded cylindrical pin profile.

Table 1 Chemical composition of the base materials

Materials	Si	Fe	Cu	Mg	Mn	Cr	Zn	Ti	Ni	Al
AA6061-T651	0.56	0.30	0.17	1.03	0.12	0.11	0.08	0.03	-	Bal.
AZ31B	0.005	0.002	0.001	Bal.	0.29	-	0.79	0.021	0.002	2.79

Table 2 Mechanical properties of base materials

Material	Tensile Strength [MPa]	Yield Strength [MPa]	Elongation [%]
AA 6061-T651	280	240	21
AZ31B	250	185	25

Friction stir welding process was performed according to the following processing conditions and parameters: 2 mm tool pin offset towards Mg side, placement of Al material in AS and Mg in RS, rotational speed, travel speed, and tilt angle set as 1070 RPM, 70 mm/min, and 3°, respectively. CFSW was conducted with additional water cooling facility, assisting the already described conventional process. The water cooling nozzle was attached behind the FSW tool as schematized in Fig. 1. The distance between tool and water cooling source and water flow rate were kept as 15 mm and 100 ml/minute respectively.

The adjoined materials were sectioned orthogonally to the welding direction to extract the specimens for microstructure analysis and microhardness measurement. A conductive thermoset resin was used to mount the specimens that, afterwards, were lapped on abrasive discs and polished on tissue discs using a polycrystalline diamond paste (0.05-9 μm). The microstructure materialized by the welding process was revealed etching the polished section using a hydrofluoric acid in water solution. Optical microscopy was carried out to appreciate the presence of eventual internal defects, then high magnification images were acquired using scanning electron microscopy (SEM), performed using a Hitachi TM3000 device. The same equipment was employed for energy dispersive X-ray spectroscopy (EDX).

The impact of microstructure modification of local mechanical properties was investigated by Vickers microhardness tests, executed according to a programmed map using a LEICA VMHT-AUTO machine. In particular, measurements were carried out along five linear and parallel patterns, separated by 1 mm each other, in the cross section of the joint, assuming the mid-thickness as reference path. The distance between two consecutive indentations, the indentation load, the loading time and indentation speed were set such as 1 mm, 100 gf (0.98 N), 15 s, and 60 μm/s respectively.

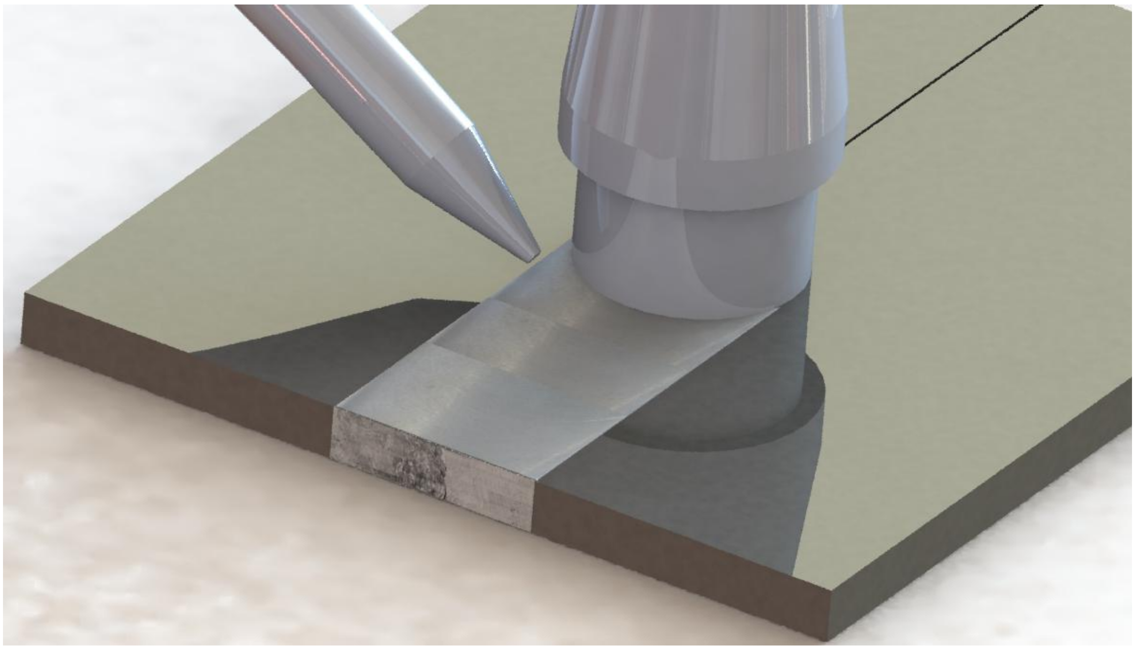

Fig. 1 – Cooling assisted friction stir welding setup

The tensile test was carried out as per the ASTM E8 standards on mini specimens of 6 mm thickness, as shown in Fig. 2. The cross head speed for the tensile test was kept as 1 mm/min. Three tensile specimens were extracted from the same weld condition coupon in order to have average values of it. Extraction of these tensile specimens was done from the middle of the specimen (Fig. 2) by wire electro discharge cutting. Ultimate tensile strength and elongation to fracture were noticed after tensile testing. Finally, X-ray diffraction analysis was performed to precisely identify the process induced IMCs.

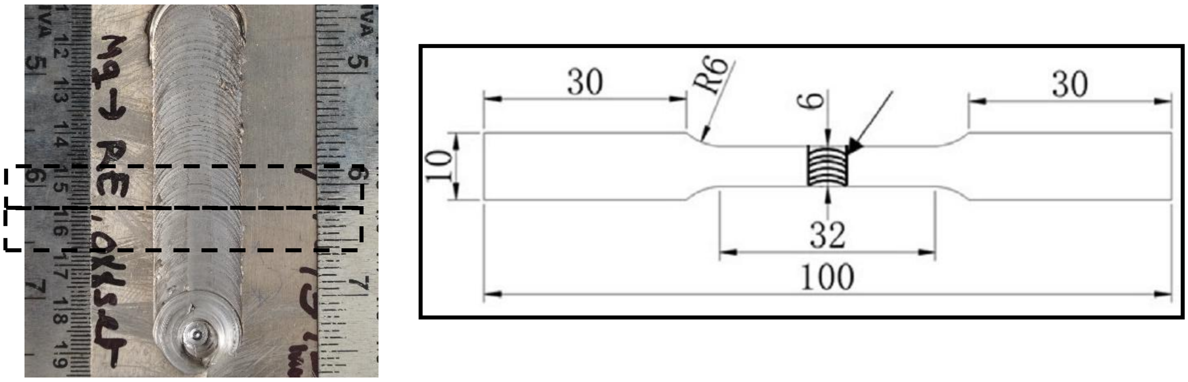

Fig. 2 – Tensile testing speciemens (ASTM E8)

3. Results and discussion

Figs. 3 (a) and (b) show the surface morphologies of Al-Mg welds produced by FSW and CFSW, respectively. Defect free surfaces are observed for both of the process conditions. Front side of stir surface is seen with rough surface having shoulder marks in case of FSW, while smooth stir surface is obtained with CFSW. Reasonably, the surface material flow is influenced by the rapid cooling action induced by the water flow that may have restricted the capability of the material to flow, resulting in a smooth stir surface. Mehta and Badheka (2017) noted similar effects for dissimilar Cu-Al FSW system.

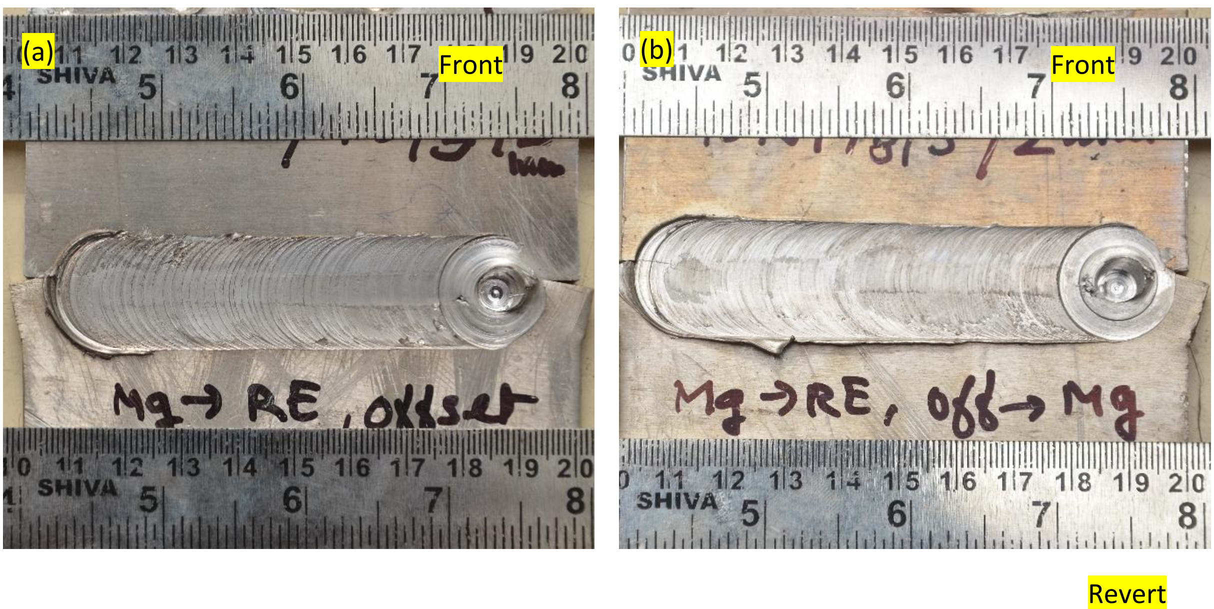

Fig. 3 – Surface morphologies (a) FSW and (b) CFSW

In Fig. 4, the macrographs of the cross sections of the two joints under investigation are reported. Both the images are built by merging more than 150 high magnification images taken in different positions in the cross section. Mishra and Mahoney (2007) mentioned four different metallurgical zones are appreciable, namely the base material (BM), the heat affected zone (HAZ), the thermo-mechanical affected zone (TMAZ), and the nugget zone (NZ). In more details, in the BM the heat input is too low to induce any microstructural variation and the parent microstructure is retained. The material in the HAZ experienced thermal cycles inducing minor changes of the microstructure (e.g. grain coarsening or a redistribution of the precipitates). In the TMAZ, the heat input, coupled with the mechanical work, produced a partially recrystallized microstructure with deformed grains. Finally a fully recrystallized microstructure with the typical onion rings is usually observed in the NZ.

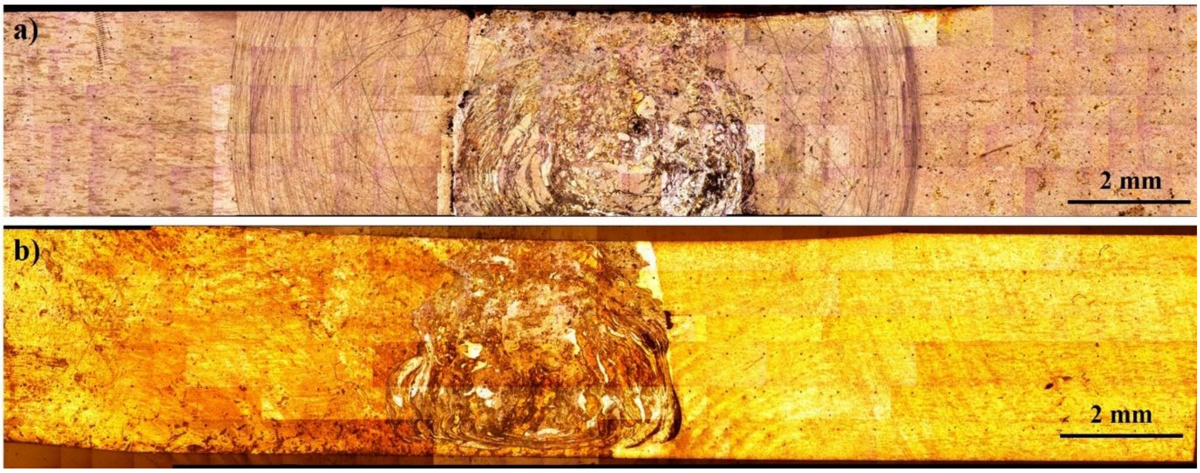

Fig. 4 – Cross section macrographs of the two joints under investigation: a) FSW; b) CFSW

In Fig. 4, the boundaries of the HAZ and TMAZ are not immediately detectable, but a clear evidence of the NZ is found. The NZ for both the joints appears very complex, due to the occurrence of a multi-material plastic flow and the formation of IMCs.

No significant defects, namely cracks or tunnel type defects, were found. The NZ exhibited a pronounced irregularly shaped region close to the weld line. The irregular shaped region has a kind of trapezoidal shape observable in the upper portion of the NZ and the weld interface near the upper surface is shifted from the initial weld centerline to the AS. It is also possible to appreciate a sharp transition between both the base materials suggesting that both alloys penetrate each other in the form of vortex and swirl like features. Zettler et al. (2006) commented similar features for Al6040-AZ31 joints. In particular, a significant mixing between the two materials was detected resulting in a complex nugget zone characterized by a trapezoidal shaped upper zone due to the dominant flow of Aluminum from the advancing side and by a bulbous region in the lower portion.

High magnification images from the different zones are provided in Fig. 5 and Fig. 6, evidencing also the location of the acquisition, aiming to better present and discuss the microstructure produced during the welding. The micrographs of the base material are also given to better discuss the microstructural changes induced.

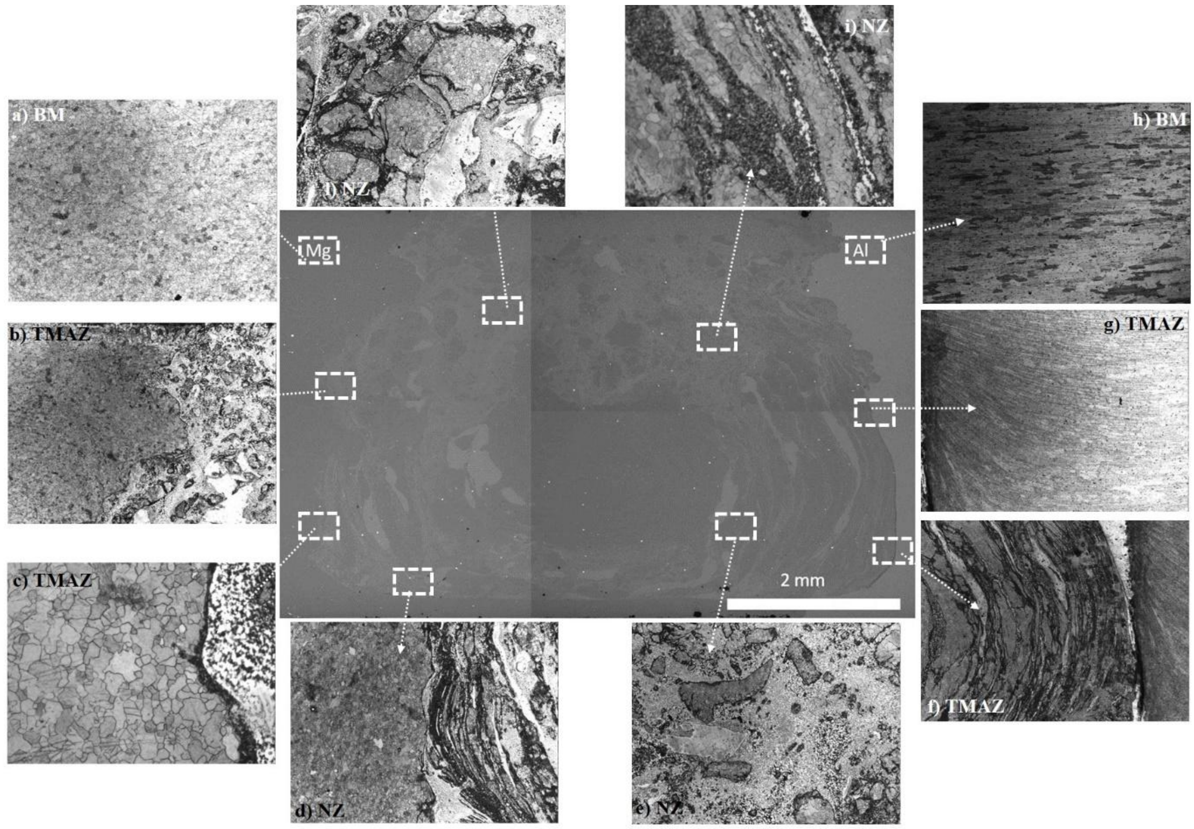

Fig. 5 – High magnification micrographs taken in the cross section of the CFSW joint: a) magnesium base material; b) magnesium side TMAZ c) magnesium side TMAZ; d) NZ; e)

NZ; f) aluminum side TMAZ; g) aluminum side TMAZ; h) aluminum base material; i) NZ; l) NZ. The central SEM low magnification image highlights the locations of each acquisition.

In the aluminum BM (Fig. 5h), the pancake-like microstructure, with stretched grains along the rolling direction, is evidenced. Some second phase black particles are appreciable as well. The presence of these particles is due to the heat treatment that leaded to the formation of precipitates, i.e. the above mentioned second phase black particles. The microstructure of the BM in the magnesium side (Fig. 5a) appears as homogenous and made of equiaxed grains, with mean dimension of approximately 15 microns. The precise identification of the HAZs is very challenging; indeed, only in the aluminum an evidence of its presence is found in the slight redistribution of the precipitates. In Fig. 5g the TMAZ on the aluminum side is reported. Highly deformed and stretched grains are clearly visible, congruently with the proximity to the stirred material in the NZ. Fig. 5f highlights the boundary region between the NZ and the TMAZ - Al side. These two regions seem to be separated by a diffusion layer. Moreover, in the NZ some onion rings are visible, made of mixed structures and IMCs. The lamellar like bands rich in aluminum and magnesium were also described and discussed by Azizieh et al. (2016) in their paper studying the dissimilar FSW of AZ31 to AA 1050. The authors argued that the different thickness observed in the rings is probably due to the mismatching of the flowability of the two materials. Concerning the TMAZ magnesium side (Fig. 5b), a completely different microstructure can be observed: the grains appear undeformed and retaining the parent microstructure. The difference between the TMAZ Mg side and the TMAZ Al side was also discussed by Kostka et al. (2009) for the AA6040 and AZ31 FSW.

Looking at Figures 5d,e,i,l, (taken in the NZ), it is possible to observe presence of magnesium, probably removed by the pin from the TMAZ (Mg side) and drown inside the NZ, as a consequence of the flow continuously promoted by the rotating pin. The complex microstructure, quite different with respect to Al and Mg similar FSW, observed in the NZ well reflects the remarkable chemical affinity of Al and Mg and their inclination to form IMCs. Indeed, the NZ is mainly constituted by Al-Mg solutions within recrystallized grains, retaining also Mg pieces with the microstructure of the parent material. Besides, several phenomena affecting the microstructure, such as intercalated lamellar structure reported by Yan et al. (2005), vortex intercalated band type structure observed by Zettler et al. (2006) and equiaxed banned structure mentioned by Yan et al. (2010) can be hypothesized, as further described and discussed hereinafter on the base of SEM and XRD observations. Within the central picture, depicting the weld bead, it is possible to observe some swirls and vortices produced by the complex material flow induced by the process, as proved and explained in Malarvizhi and Balasubramanian (2012). The interfaces between the different metallurgical zones are tortuous and with some interpenetrating features (IPF). Venkateswaran and Reynolds (2012) observed and discussed these results. The authors argued that the type of the interface is dictated by the adopted welding parameters and, in particular, the interface characterized by IPF (clearly visible in Fig. 5) are promoted by high rotational speeds (usually above the 900 rpm). The slight asymmetry of the IPF can be ascribed to the offset of the pin in the retreating side.

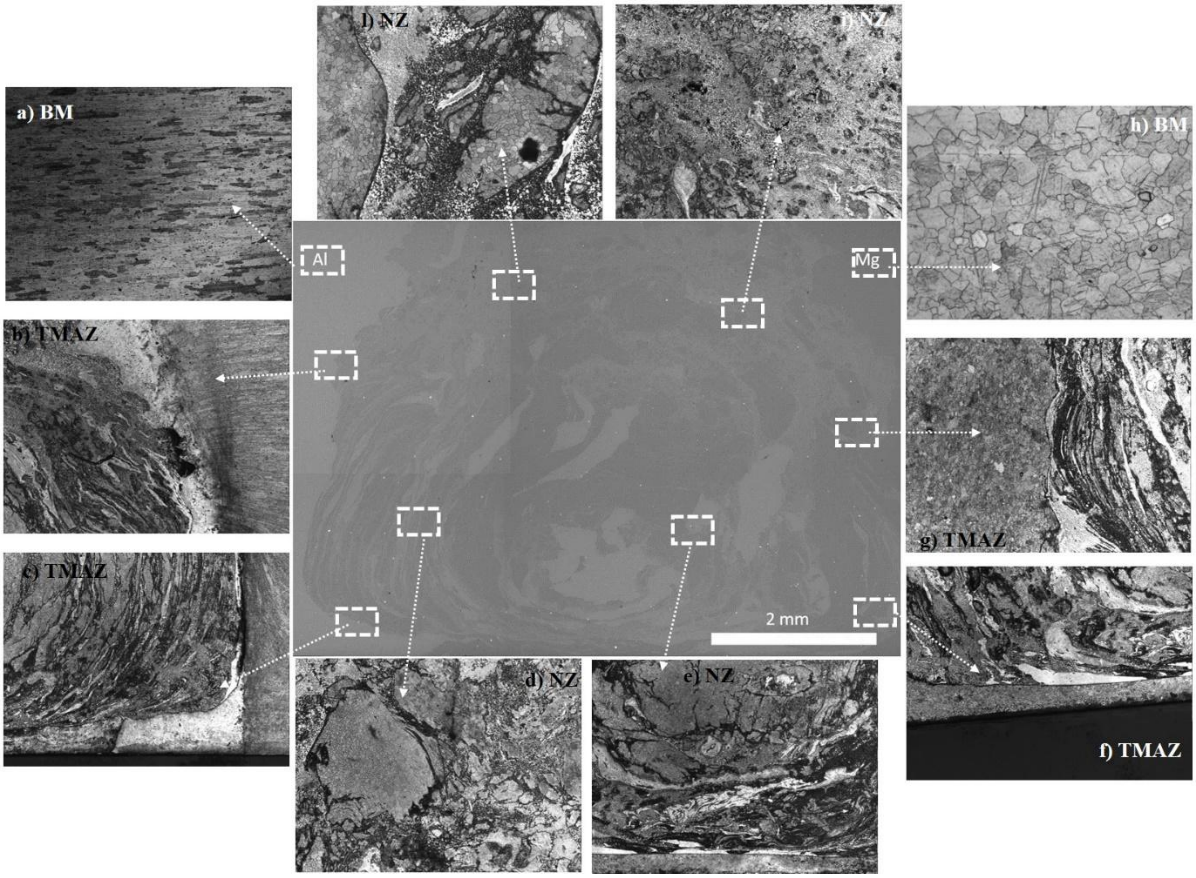

Fig. 6 – High magnification micrographs taken in the cross section of the FSW joint: a) aluminum base material; b) aluminum side TMAZ c) aluminum side TMAZ; d) NZ; e) NZ; f) magnesium side TMAZ; g) magnesium side TMAZ; h) magnesium base material; i) NZ; l) NZ. The central SEM low magnification image highlights the locations of each acquisition.

Fig. 6 reports the microstructure of the FSW joint. Qualitatively, similar observations, as already drawn for the CFSW (see Fig. 5) joint, can be pointed out, being the main significant difference given by the presence of some little cracks in the bond area between the TMAZ (Al side) and the NZ. Such cracks are clearly appreciable in Figs. 6b and 6c.

Detailed SEM observations with EDX analysis are reported below in Fig. 7 and Table 3, respectively. In particular, Fig. 7 details the interface region between the NZ and the TMAZ (Al side) as captured by high magnification SEM. EDX measurements, whose outcomes are summarized in Table 3, are carried out in the locations highlighted within the picture. As can be seen, a diffusion layer is clearly visible, identified as a solid solution of Mg in an Al matrix, between the NZ and the TMAZ (Al side).

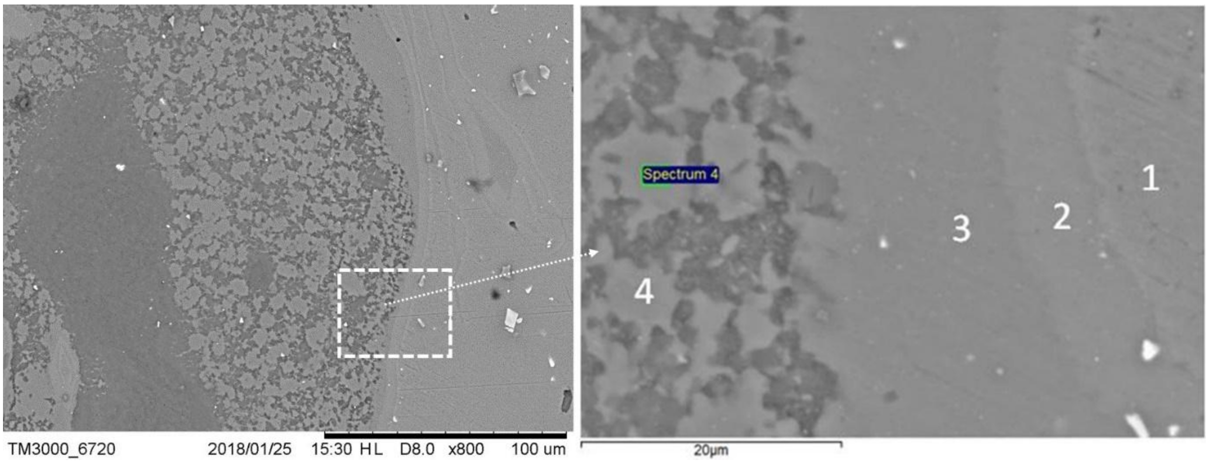

Fig. 7- SEM images of the interface between NZ and TMAZ at the Al side (CFSW joint).

Table 3 – EDX results in the locations highlighted in Fig. 7.

Zone	Chemical composition (wt %)					Interpretation	Location
	O	Mg	Al	Si	Zn		
1	3.443	13.057	83.099	0.401	-	Solid solution of Mg in Al matrix	Transition between NZ and TMAZ Al side
2	3.578	38.536	57.682	0.204	-	Phase β (Al_3Mg_2)	NZ
3	3.909	49.629	46.150	0.313	-	Phase γ ($Al_{12}Mg_{17}$)	NZ
4	4.404	55.902	39.009	-	0.684	Phase γ ($Al_{12}Mg_{17}$)	NZ

On the other hand, no diffusion layer is detected at the transition between the NZ and the TMAZ (Mg side), as shown in Fig. 8. It suggests that different phenomena occurred on the Al side and on the Mg side.

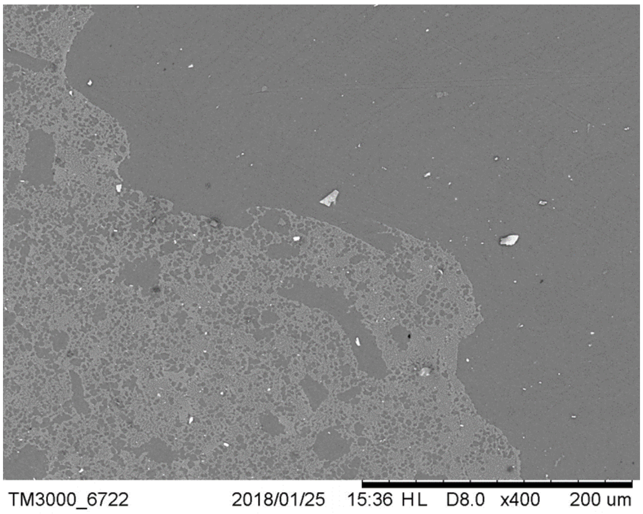

Fig. 8 –SEM images of the transition between the NZ and the TMAZ at the Mg side (CFSW joint).

The microstructure established in the NZ of the CFSW joint can be assimilated to a metal matrix composites with variable composition moving from the AS (Al side) toward the RS (Mg side). More specifically, a Mg solution in an Al matrix can be identified in the former case (Al side), while an Al solution in a Mg matrix can be observed in the other region. In both cases, IMCs are copiously distributed, as highlighted in the following images and tables, generating also an onion ring structure, confirmed by the SEM (Fig. 9) and EDX analysis (Table 4) reported below.

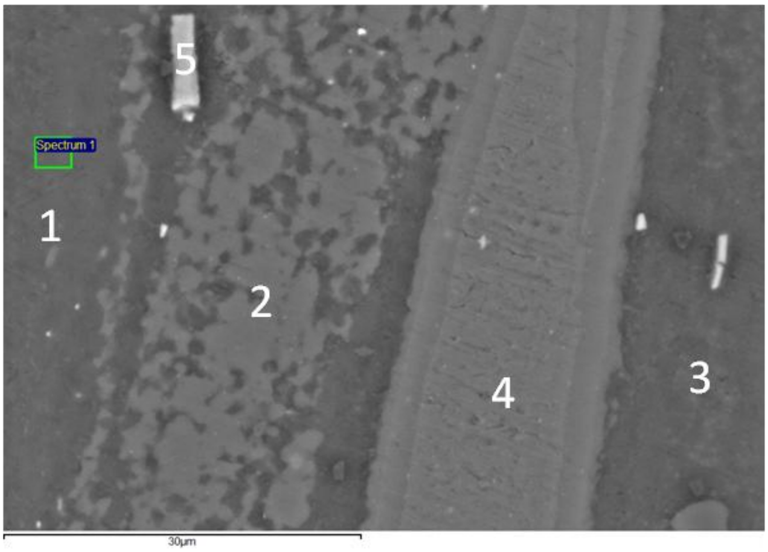

Fig. 9 – SEM images of the NZ of joint CFSW, indicating the locations of the EDX analysis.

Table 4 – EDX results in the locations highlighted in Fig. 9.

Zone	Chemical composition detected (wt %)						Interpretation
	O	Mg	Al	Si	Mn	Zn	
1	5.271	74.494	19.634	-	-	0.601	Solid solution of Al in Mg matrix
2	4.674	56.378	38.337	-	-	0.611	Phase γ ($Al_{12}Mg_{17}$)
3	7.868	72.918	18.390	0.166	-	0.657	Solid solution of Al in Mg matrix
4	4.144	15.214	80.296	0.346	-	-	Solid solution of Mg in Al matrix
5	14.800	33.687	34.205	0.355	16.953	-	$Al(Mg)_4Mn)$ IMC coming from the Mg

In case of FSW joint, the formation of IMCs and solid solution phases in the corresponding base material phases are observed, in line with what was observed in CFSW joint in terms of phase identifications, as evidenced by SEM (Fig. 10) and EDX analysis (Table 5) inside the NZ. However, the amount of IMCs formed may be different depending on the processing conditions. The volume fractions of IMCs are expected to be relatively higher in case of the joint welded by conventional FSW.

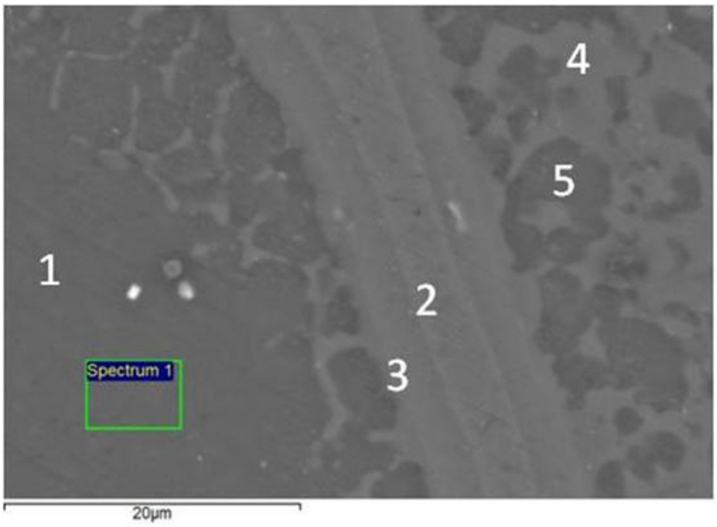

Fig. 10 – SEM images of the NZ and TMAZ (Al side) of FSW joint, highlighting the locations of the EDX analysis.

Table 5 – EDX results in the locations highlighted in Fig. 10.

Zone	Chemical composition detected (wt %)						Interpretation
	O	Mg	Al	Si	Mn	Zn	
1	4.223	86.137	8.717	-	-	0.924	Solid solution of Al in Mg matrix
2	3.712	22.520	73.505	0.264	-	-	Solid solution of Mg in Al matrix
3	3.622	50.642	45.585	0.151	-	-	Phase β (Al_3Mg_2)
4	3.767	65.130	30.456	-	-	0.647	Phase γ ($Al_{12}Mg_{17}$)
5	3.650	79.016	17.334	-	-	-	Solid solution of Al in Mg matrix

The diffractogram presented in Fig. 11, obtained from the XRD analysis of the NZ, proves that the NZ is made of Al, Mg beta phase and gamma phase. Furthermore, it univocally identifies the IMCs phases, whose presence is indicated also by the EDX investigation, as given by $Al_{12}Mg_{17}$ and Al_3Mg_2, in agreement with the analyses of Venkateswaran and Reynolds (2012) and Shi et al. (2017). The authors also observed that the presence of IMCs in the weld interface including IPF detrimentally affects the mechanical properties of the joints being a preferential path for the crack propagation during the loading of the structure. As far the IMCs phases nucleation, Kostka et al. (2009) and Fu et al. (2015) argued that such IMCs are formed because of solid state diffusion and constitutional liquation (or eutectic) mechanisms. The former occurred usually in case of low heat input during the FSW because the welding temperature usually remains below the eutectic temperatures of the Al-Mg binary phases (i.e. 437°C in the Mg dominant side and 450°C in the Al side) and thus the compounds nucleated and grew by means atoms diffusion between aluminum and magnesium. On the other hand, the authors indicated the constitutional liquation as the main factor in the formation of IMCs. Indeed, the heat generated by the friction between materials and tool during the stirring action and the material plastic deformation allows the weld zone to reach the eutectic lines. Therefore, local melting can occur forming a liquid film along the grain boundary allowing a more rapid diffusion of Al and Mg atoms and the subsequent rapid solidification produce the observed microstructure according the eutectic reactions:

$$Al\ (450°C): L \rightarrow Al_3Mg_2$$

$$Mg\ (437°C): L \rightarrow Al_{12}Mg_{17}$$

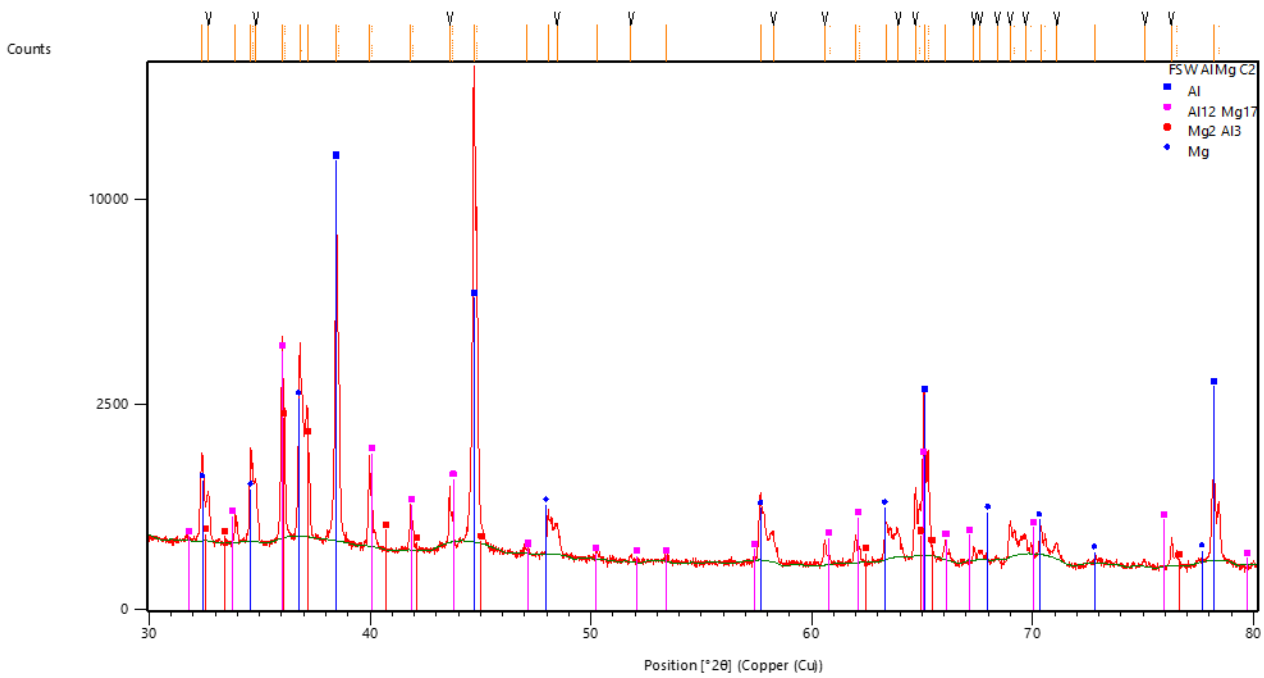

Fig. 11 – Diffractogram obtained in the NZ of the CFSW joint. Identical results were obtained in the case of standard FSW, so this image can be assumed as representative of both processing conditions.

The tensile strength and elongation measurements are presented in Fig. 12. Tensile strength of 128 MPa and 182 MPa are obtained for Al-Mg welds produced by FSW and CFSW respectively. The reason for the lower tensile strength of FSW joint is attributable to the formation of some cracks at the interface between NZ and TMAZ (Fig. 16). Similar cracks are not noticed in CFSW joint. Mofid et al. (2012b) mentioned that brittle form of IMCs is a major reason for the crack, because the fracture preferentially propagated along the brittle intermetallic layers, as confirmed by the cleavage-type fracture surfaces observed. On the other hand, in the same work the authors claimed that underwater friction stir welding presents a ductile fracture surface, pointing out a reduced amount of IMCs formed during the weld. There are no defects reported in the detailed analysis of microstructure examinations of CFSW. The amount of IMCs in case of FSW joint is less than the CFSW joint, based on studies by Mofid et al. (2012b) and Mofid et al. (2012a). Therefore, improvement in tensile strength is achieved with the CFSW relative to FSW.

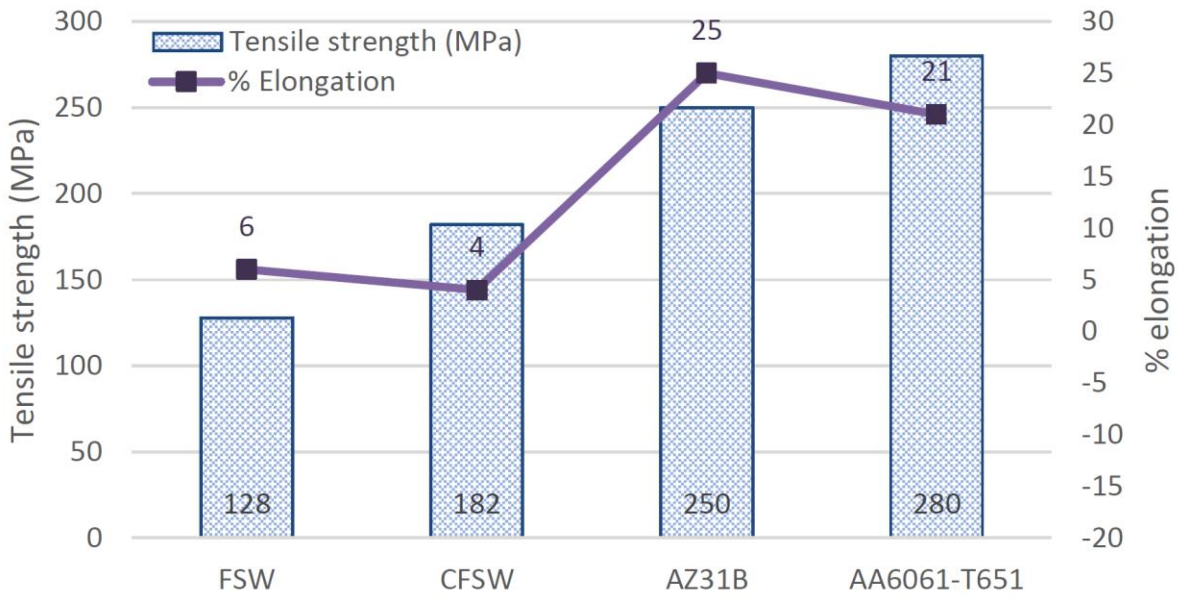

Fig. 12 – Tensile properties of welds and base materials and images of the broken specimens.

Low percentage of elongation is reported for both of the welds of FSW and CFSW, if compared to the base materials. Large amount of IMCs, precipitates and different phases, identified in above analysis, are responsible for the low percentage of elongation of both the joints. Shi et al. (2017) demonstrated that the mechanical properties of the joints are ruled by the IMCs and the chemical composition, size and distribution of the above mentioned IMCs are in turn regulated by the processing conditions. The CFSW failed on the boundary of the weld bead: both the specimens showed a fragile fracture, suggested also by the low values of the elongation measured. Concerning the tensile tests carried out on the parent materials, a typical ductile fracture with necking occurrence was observed.

The ultimate tensile strength (UTS) values measured for the CFSW joints are close to the 73% to the ones of the AZ31B base material; to make a comparison Fu et al. (2015) in their work on the FSW of AA 6061 and AZ31 obtained an UTS close to the 70% of the Mg parent material and Yan et al. (2005) in their paper studying the FSW of AA 1060 and AZ31 obtained a joint with an UTS close to the 67% of the Al one. The samples showed a brittle fracture probably induced by the fragile IMCs. Dorbane et al. (2016) provided similar results, reporting that the conventional FS welded joints exhibit a very low joint efficiency (evaluated as the ratio of the UTS of the Al-Mg welded samples and the UTS of parental weaker parental material) between 18% and 55% depending the process parameters.

Photographs of the tested specimens, one for each sample (namely FSW, CFSW, Al parent material and Mg base material), are given in figure 13. As appreciable, both the CFSW and FSW samples failed on the Al side of the joint while the Al base material, as expected, showed a more ductile behavior. Concerning the welded sample, the failure location was observed in the middle of the Al-Mg mixed area for FSW samples, while the CFSW samples failed on the boundary of this region on the aluminum side.

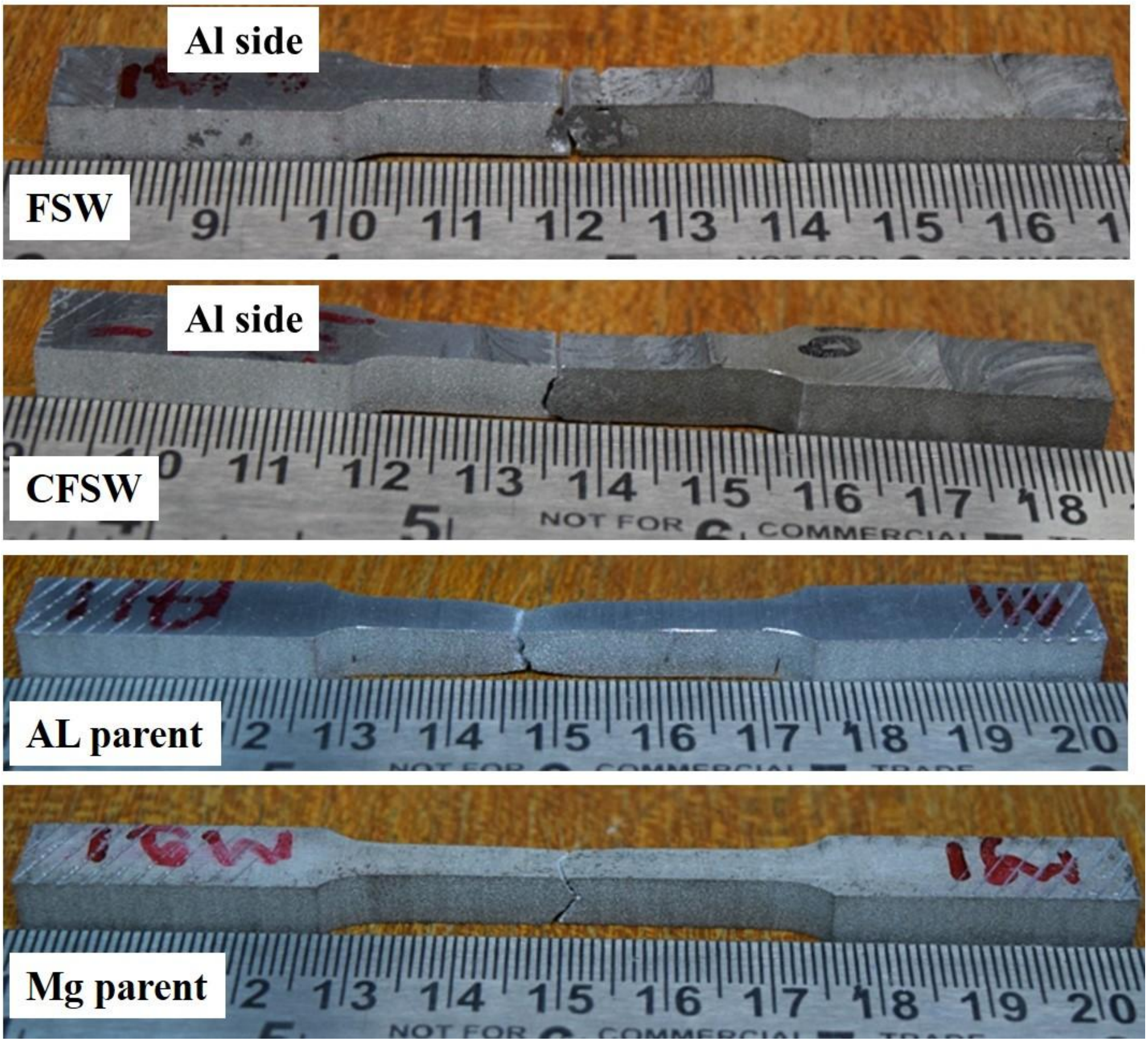

Fig. 13 – Photographs of the tested specimens, one for each sample tested.

High magnification SEM micrographs of the fracture surfaces for the FSW and CFSW specimens are showed, respectively, in figures 14 and 15.

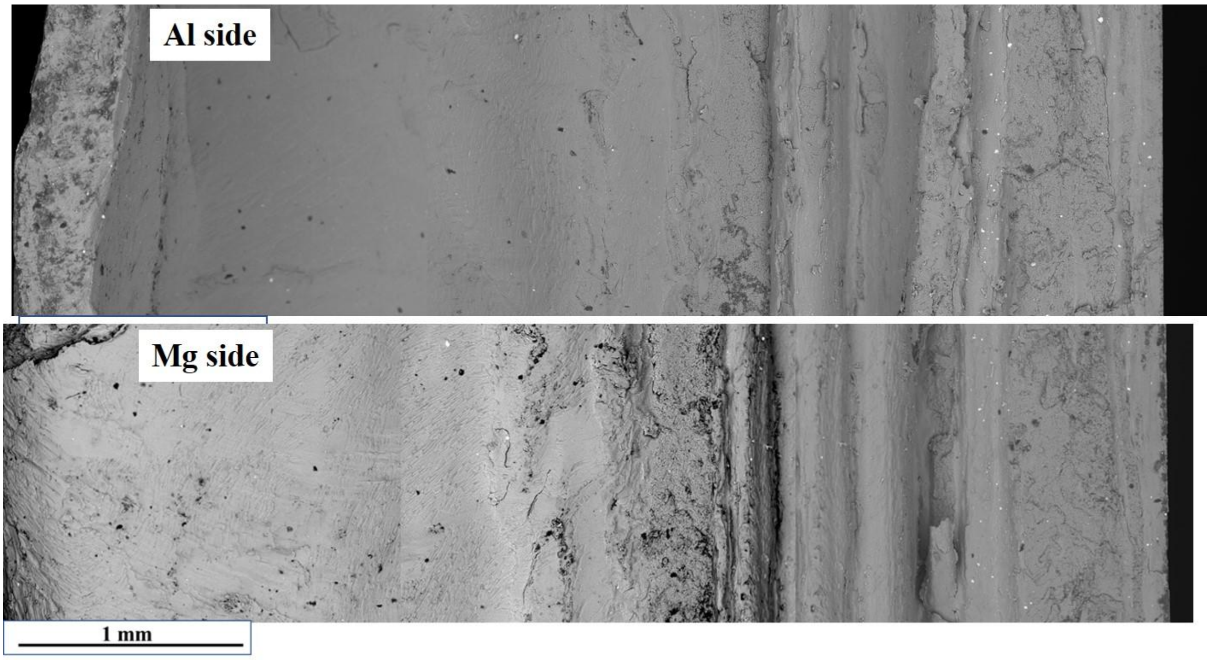

Fig. 14 – High magnification SEM micrographs of the fracture surfaces of the FSW joint.

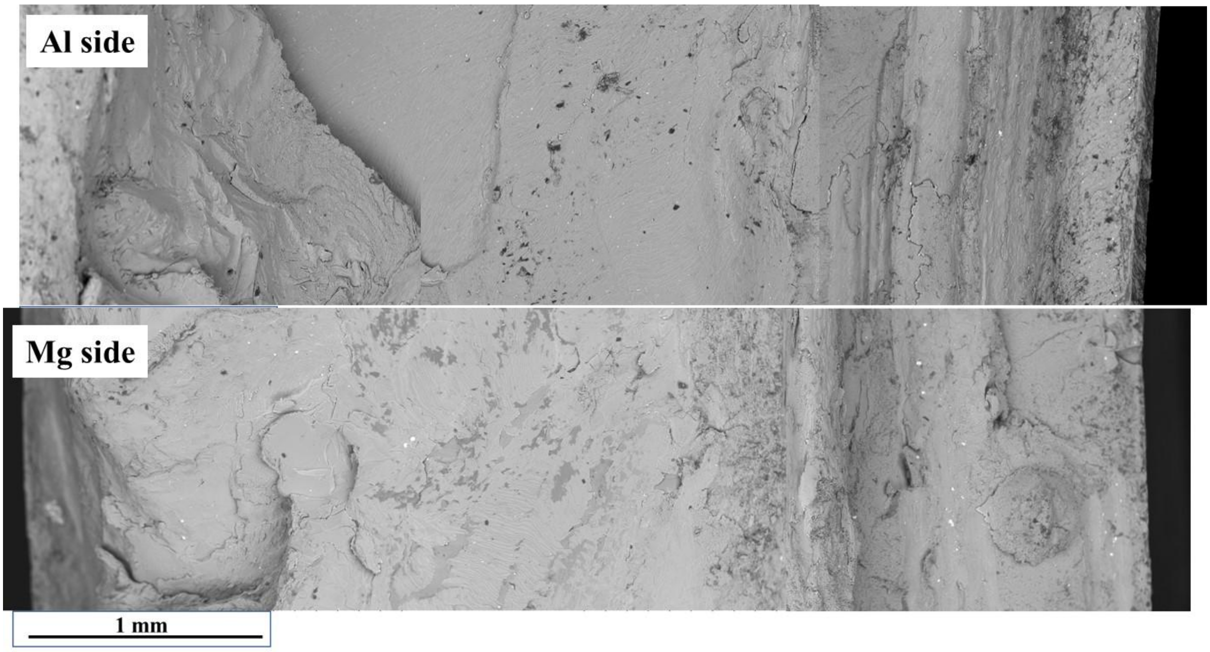

Fig. 15 – High magnification SEM micrographs of the fracture surfaces of the CFSW joint.

The SEM analysis of the failure surfaces highlighted some differences in the rupture mode between the differently welded joints, whereas the FSW samples exhibited a prevalently brittle failure mode due to the higher amount of IMCs.

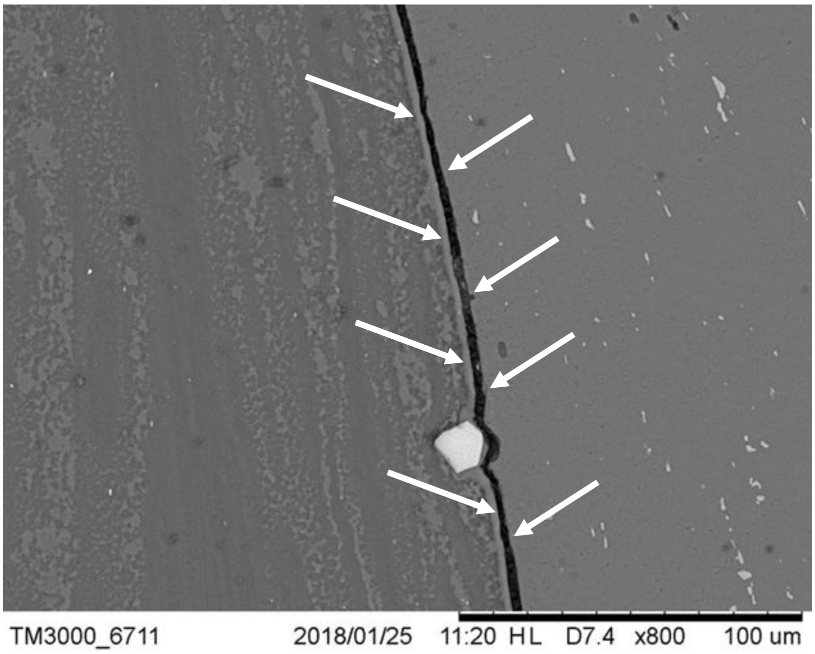

Fig. 16 – High magnification SEM micrograph of a crack between the NZ and the TMAZ Al side (FSW joint).

Fig. 17 and Fig. 18 present the micro hardness distribution measured in FSW and CFSW joints, respectively. NZ consists of very high hardness compare to Al and Mg base materials in both the process conditions. The high values observed are mainly due to the presence of IMCs in the NZ. Highest peak of 298 HV is reported for CFSW joint in the NZ (Fig. 18). The maximum peak of hardness in case of FSW joint is 204 HV (Fig. 17). This shows the presence of IMC only at that particular location, which has resulted into such high hardness values. It confirms that amount of IMCs formed are maximum in case of FSW joint compared to the CFSW joint. The cooling effect may have reduced the amount of IMCs. Mofid et al. (2012a) and Mehta and Badheka (2017) reported similar results of IMCs by having additional cooling effects in FSW. The authors observed a hardness values in the stir zone not much higher than the parental metals pointing out a reduced formation of IMCs in the cooled assisted FSW w.r.t. the conventional FSW.

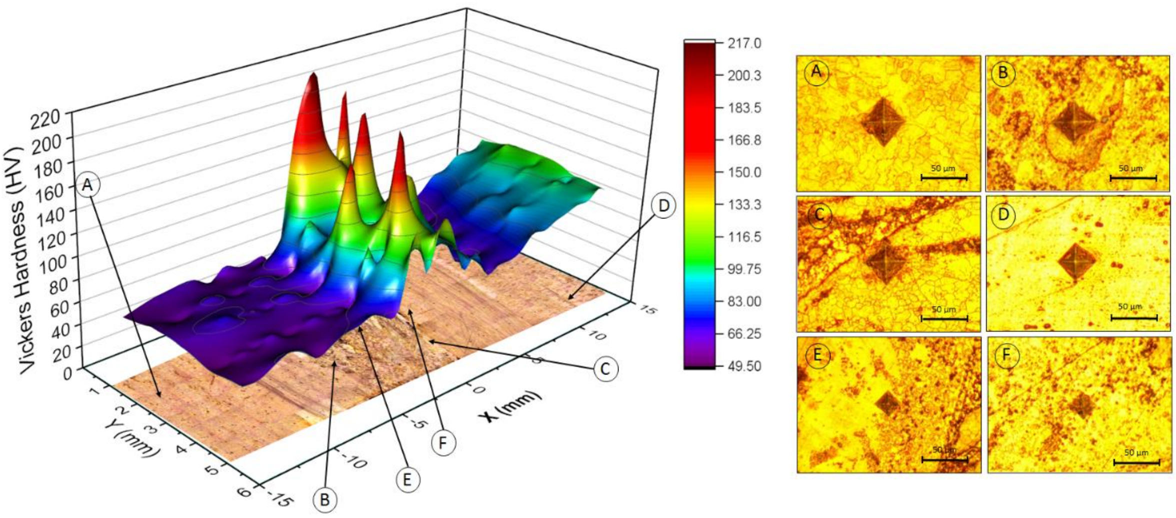

Fig. 17 - Microhardness distribution for FSW joint, including some representative indentations (A: Mg base material – HV 64.8; B, C: nugget zone – HV 69.9, 89.5; D: Al base material – HV 95.7; E, F: IMCs in the nugget zone – HV 199, 204)

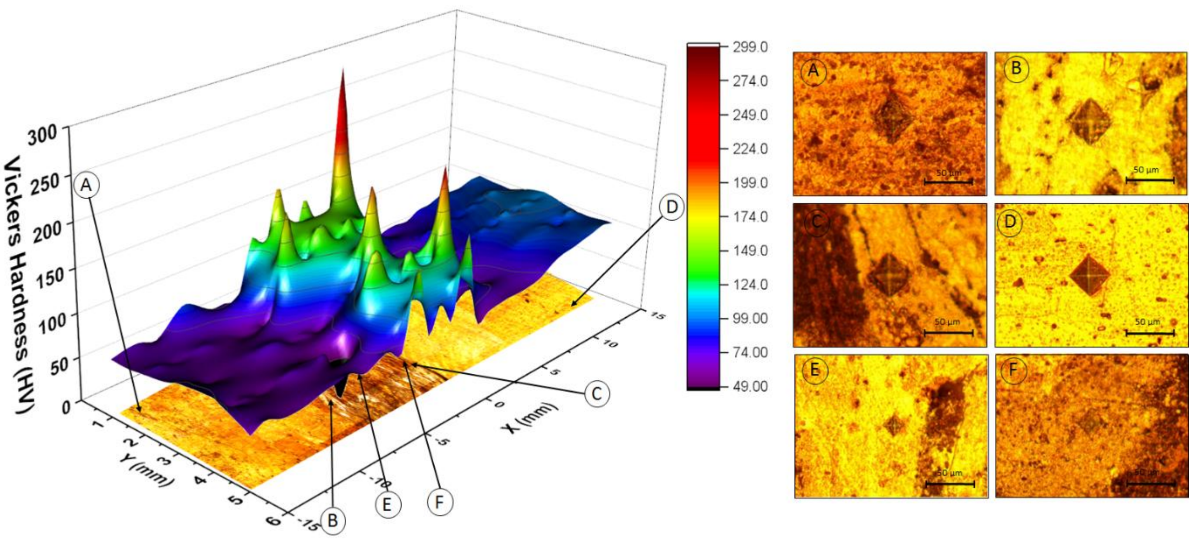

Fig. 18 - Microhardness distribution for CFSW joint, including some representative indentations (A: Mg base material – HV 66.1; B, C: nugget zone – HV 138, 77.6; D: Al base material – HV 93.8; E, F: IMCs in the nugget zone – HV 298,159)

4. Conclusions

- The mechanical properties, namely tensile strength and micro hardness of dissimilar Al-Mg joints are enhanced by CFSW relative to FSW joints. The tensile strength of 182 MPa is reported for CFSW joint while 128 MPa is reported for FSW joint.

- The CFSW presents a higher joint efficiency of approximately 73%, than the conventional FSW, which provides a value of 51%, that is in agreement with the values commented in the dedicate literature, proving the effectiveness of the suggested method.
- NZ is reported with onion rings composed of phases such as Mg in an Al matrix, Al in an Mg matrix, Al_3Mg_2, and $Al_{12}Mg_{17}$.
- A diffusion layer, identified as a solid solution of Mg in an Al matrix, was observed between the NZ and the TMAZ at the Al side, while no diffusion layer was detected between NZ and TMAZ at the Mg side.
- Maximum hardness peaks are reported in the NZ of FSW joint relative to CFSW joint. Higher average hardness values were measured in the NZ of the FSW joint suggesting the formation of a significant amount of IMCs. Cooling assisted friction stir weld is characterized by lower hardness. Isolated highest peaks can be observed only at specific locations.

Acknowledgements

The authors would like to thank the Institute of Engineers, India for providing funding (Project ID : RDUG2017010) for the present investigations.

Data availability statement

The authors declare that the raw data required to reproduce these findings are available to download from [INSERT PERMANENT WEB LINK(s)]. The processed data required to reproduce these findings are available to download from [INSERT PERMANENT WEB LINK(s)].

References

Atabaki, M.M., Nikodinovski, M., Chenier, P., Ma, J., Harooni, M., Kovacevic, R., 2014. Welding of Aluminum Alloys to Steels: An Overview. J. Manuf. Sci. Prod. 14, 59–78. https://doi.org/10.1515/jmsp-2014-0007

Azizieh, M., Sadeghi Alavijeh, A., Abbasi, M., Balak, Z., Kim, H.S., 2016. Mechanical properties and microstructural evaluation of AA1100 to AZ31 dissimilar friction stir welds. Mater. Chem. Phys. 170, 251–260.

https://doi.org/10.1016/j.matchemphys.2015.12.046

Bang, H., Bang, H., Jeon, G., Oh, I., Ro, C., 2012. Gas tungsten arc welding assisted hybrid friction stir welding of dissimilar materials Al6061-T6 aluminum alloy and STS304 stainless steel. Mater. Des. 37, 48–55. https://doi.org/10.1016/j.matdes.2011.12.018

Bang, H., Bang, H., Song, H., Joo, S., 2013. Joint properties of dissimilar Al6061-T6 aluminum alloy/Ti–6%Al–4%V titanium alloy by gas tungsten arc welding assisted hybrid friction stir welding. Mater. Des. 51, 544–551. https://doi.org/10.1016/j.matdes.2013.04.057

Chang, W.-S., Rajesh, S.R., Chun, C.-K., Kim, H.-J., 2011. Microstructure and Mechanical Properties of Hybrid Laser-Friction Stir Welding between AA6061-T6 Al Alloy and AZ31 Mg Alloy. J. Mater. Sci. Technol. 27, 199–204. https://doi.org/10.1016/S1005-0302(11)60049-2

DebRoy, T., Bhadeshia, H.K.D.H., 2010. Friction stir welding of dissimilar alloys – a perspective. Sci. Technol. Weld. Join. 15, 266–270. https://doi.org/10.1179/174329310X12726496072400

Dorbane, A., Mansoor, B., Ayoub, G., Shunmugasamy, V.C., Imad, A., 2016. Mechanical, microstructural and fracture properties of dissimilar welds produced by friction stir welding of AZ31B and Al6061. Mater. Sci. Eng. A 651, 720–733. https://doi.org/10.1016/j.msea.2015.11.019

Fu, B., Qin, G., Li, F., Meng, X., Zhang, J., Wu, C., 2015. Friction stir welding process of dissimilar metals of 6061-T6 aluminum alloy to AZ31B magnesium alloy. J. Mater. Process. Technol. 218, 38–47. https://doi.org/10.1016/j.jmatprotec.2014.11.039

Ji, S., Huang, R., Meng, X., Zhang, L., Huang, Y., 2017a. Enhancing Friction Stir Weldability of 6061-T6 Al and AZ31B Mg Alloys Assisted by External Non-rotational Shoulder. J. Mater. Eng. Perform. 26, 2359–2367. https://doi.org/10.1007/s11665-017-2640-8

Ji, S., Meng, X., Liu, Z., Huang, R., Li, Z., 2017b. Dissimilar friction stir welding of 6061 aluminum alloy and AZ31 magnesium alloy assisted with ultrasonic. Mater. Lett. 201, 173–176. https://doi.org/10.1016/j.matlet.2017.05.011

Joo, S., 2013. Joining of dissimilar AZ31B magnesium alloy and SS400 mild steel by hybrid gas tungsten arc friction stir welding. Met. Mater. Int. 19, 1251–1257. https://doi.org/10.1007/s12540-013-6016-9

Kostka, A., Coelho, R.S., dos Santos, J., Pyzalla, A.R., 2009. Microstructure of friction stir welding of aluminium alloy to magnesium alloy. Scr. Mater. 60, 953–956. https://doi.org/10.1016/j.scriptamat.2009.02.020

Liu, X., Lan, S., Ni, J., 2015. Electrically assisted friction stir welding for joining Al 6061 to TRIP 780 steel. J. Mater. Process. Technol. 219, 112–123. https://doi.org/10.1016/j.jmatprotec.2014.12.002

Liu, Z., Meng, X., Ji, S., Li, Z., Wang, L., 2018. Improving tensile properties of Al/Mg joint by smashing intermetallic compounds via ultrasonic-assisted stationary shoulder friction stir welding. J. Manuf. Process. 31, 552–559. https://doi.org/10.1016/j.jmapro.2017.12.022

Lv, X., Wu, C., Yang, C., Padhy, G.K., 2018. Weld microstructure and mechanical properties in ultrasonic enhanced friction stir welding of Al alloy to Mg alloy. J. Mater. Process. Technol. 254, 145–157. https://doi.org/10.1016/j.jmatprotec.2017.11.031

Malarvizhi, S., Balasubramanian, V., 2012. Influences of tool shoulder diameter to plate thickness ratio (D/T) on stir zone formation and tensile properties of friction stir welded dissimilar joints of AA6061 aluminum–AZ31B magnesium alloys. Mater. Des. 40, 453–460. https://doi.org/10.1016/j.matdes.2012.04.008

Mehta, K.P., Badheka, V.J., 2017. Hybrid approaches of assisted heating and cooling for friction stir welding of copper to aluminum joints. J. Mater. Process. Technol. 239, 336–345. https://doi.org/10.1016/j.jmatprotec.2016.08.037

Mishra, R.S., Mahoney, M.W., 2007. Friction Stir Welding and Processing, 1 edition. ed. ASM International.

Mofid, M.A., Abdollah-Zadeh, A., Ghaini, F.M., Gür, C.H., 2012a. Submerged friction-stir welding (SFSW) underwater and under liquid nitrogen: An improved method to join Al alloys to Mg alloys. Metall. Mater. Trans. A Phys. Metall. Mater. Sci. 43, 5106–5114. https://doi.org/10.1007/s11661-012-1314-2

Mofid, M.A., Abdollah-zadeh, A., Malek Ghaini, F., 2012b. The effect of water cooling during dissimilar friction stir welding of Al alloy to Mg alloy. Mater. Des. 36, 161–167.

https://doi.org/10.1016/j.matdes.2011.11.004

Safi, S.V., Amirabadi, H., Besharati Givi, M.K., Safi, S.M., 2016. The effect of preheating on mechanical properties of friction stir welded dissimilar joints of pure copper and AA7075 aluminum alloy sheets. Int. J. Adv. Manuf. Technol. 84, 2401–2411. https://doi.org/10.1007/s00170-015-7877-5

Shah, L.H., Ishak, M., 2014. Review of Research Progress on Aluminum–Steel Dissimilar Welding. Mater. Manuf. Process. 29, 928–933. https://doi.org/10.1080/10426914.2014.880461

Shah, L.H., Othman, N.H., Gerlich, A., 2018. Review of research progress on aluminium–magnesium dissimilar friction stir welding. Sci. Technol. Weld. Join. 23, 256–270. https://doi.org/10.1080/13621718.2017.1370193

Shi, H., Chen, K., Liang, Z., Dong, F., Yu, T., Dong, X., Zhang, L., Shan, A., 2017. Intermetallic Compounds in the Banded Structure and Their Effect on Mechanical Properties of Al/Mg Dissimilar Friction Stir Welding Joints. J. Mater. Sci. Technol. 33, 359–366. https://doi.org/10.1016/j.jmst.2016.05.006

Simar, A., Avettand-Fènoël, M.N., 2017. State of the art about dissimilar metal friction stir welding. Sci. Technol. Weld. Join. 22, 389–403. https://doi.org/10.1080/13621718.2016.1251712

Venkateswaran, P., Reynolds, A.P., 2012. Factors affecting the properties of Friction Stir Welds between aluminum and magnesium alloys. Mater. Sci. Eng. A 545, 26–37. https://doi.org/10.1016/j.msea.2012.02.069

Yaduwanshi, D.K., Bag, S., Pal, S., 2016. Numerical modeling and experimental investigation on plasma-assisted hybrid friction stir welding of dissimilar materials. Mater. Des. 92, 166–183. https://doi.org/10.1016/j.matdes.2015.12.039

Yan, J., Xu, Z., Li, Z., Li, L., Yang, S., 2005. Microstructure characteristics and performance of dissimilar welds between magnesium alloy and aluminum formed by friction stirring. Scr. Mater. 53, 585–589. https://doi.org/10.1016/j.scriptamat.2005.04.022

Yan, Y., Zhang, D.T., Qiu, C., Zhang, W., 2010. Dissimilar friction stir welding between 5052 aluminum alloy and AZ31 magnesium alloy. Trans. Nonferrous Met. Soc. China (English Ed. 20, 2–6. https://doi.org/10.1016/S1003-6326(10)60550-X

Zettler, R., Da Silva, A.A.M., Rodrigues, S., Blanco, A., Dos Santos, J.F., 2006. Dissimilar Al to Mg alloy friction stir welds. Adv. Eng. Mater. 8, 415–421. https://doi.org/10.1002/adem.200600030

Zhao, Y., Lu, Z., Yan, K., Huang, L., 2015. Microstructural characterizations and mechanical properties in underwater friction stir welding of aluminum and magnesium dissimilar alloys. Mater. Des. 65, 675–681. https://doi.org/10.1016/j.matdes.2014.09.046

Conventional and cooling assisted friction stir welding of AA6061 and AZ31B alloys

Kush P Mehta[1], Pierpaolo Carlone[2], Antonello Astarita[3], Fabio Scherillo[3], Felice Rubino[2], Poojan Vora[1]

[1]Department of Mechanical Engineering, School of Technology (SOT), Pandit Deendayal Petroleum University (PDPU), Raisan, Gandhinagar 382007, Gujarat, India.

[2]Department of Industrial Engineering, University of Salerno, Via Giovanni Paolo II, 132, 84084, Fisciano (SA), Italy.

[3]Department of Chemical, Materials and Industrial Production Engineering, University of Naples, "Federico II", P.le Tecchio 80, 80100 Naples, Italy

Abstract

Conventional and cooling assisted friction stir welded Al-Mg joints were investigated by visual inspection, optical macro plus microscopy, scanning electron micrographs, energy dispersive X-ray spectroscopy, X-ray diffractions, tensile testing and micro hardness indentation. The nugget zone is characterized by onion rings composed of different phases such as Mg in an Al matrix, Al in an Mg matrix as well as intermetallic compounds, Al_3Mg_2 and $Al_{12}Mg_{17}$. A diffusion layer was detected on the Al side of the joint between the nugget and thermo-mechanically affected zones identifying a solid solution of Mg in Al. No diffusion layer was observed on the Mg side. The tensile strength of the dissimilar joints is enhanced by cooling assisted welding process due to the reduction in the amount of intermetallic compounds inside the weld bead. Congruently, higher hardness peaks are reported in the nugget zone of conventional FSW joint with respect to the CFSW joint.

Keywords: cooling assisted friction stir welding, dissimilar joint, mechanical properties, microstructure, intermetallic compounds

1. Introduction

Friction stir welding (FSW) is observed as qualified technique to obtain sound dissimilar joints adopting different pairs of metallic materials, such as Al-Cu, Al-Mg and Al-steel structures. Mehta and Badheka (2017) provided comprehensive investigation on joining of Aluminum (Al)-Copper (Cu) by means of FSW technology, pointing that, despite the potential benefits, the pronounced formation of intermetallic compounds due to the limited solubility of Al and Cu at room temperature lowers the quality of the joints. The authors concluded that novel variations in the conventional FSW were proved to be able to enhance the performances of the Al-Cu system. Shah et al. (2018) reviewed the bonding mechanisms of FS welded Al-Magnesium (Mg). The authors stated that the heat dissipated in the material during the process significantly affects the amount of intermetallic compounds (IMCs) from the welding process. In particular, process parameters such as base metal positioning, tool offset and revolutionary pitch (defined as ratio between and tool welding and rotational speeds) dictate the heat input, ruling the Al-Mg joint interface and the joint efficiency. Suppression of excessive heat showed to be a promising solution to limit the IMC growth and improve the overall joint quality. Shah and Ishak (2014) and Atabaki et al. (2014) pointed out the relevance of the welding parameters synergy to control type, size and amount of Fe/Al compounds. In particular, thick layers of different intermetallic (e.g. $FeAl_3$, Fe_2Al_5 and $FeAl_2$) observed at the faying surfaces depending on the rotational speed and pin depth adopted. Preheating of welding materials with FSW technique ~~(e.g. hybrid FSW/TIG method)~~ demonstrated to be suitable strategies to overcome the limitations of conventional processes. DebRoy and Bhadeshia (2010) and Simar and Avettand-Fènoël (2017) reviewed other different dissimilar materials structure, including Al-titanium (Ti), Ti-steel, Mg-steel, and Mg-Ti summarizing the guidelines to tune-up the process parameters in order to manufacture sound and free-defects welds. The main issues that have to be addressed during a dissimilar FSW are related to: i) the different plasticisation temperatures of the metals that affect the material flow and ii) the constitutional liquation that coupled with the reciprocal affinity of metals dictates the IMC nature and distribution. As far the material flow, the authors suggest to place the softer material on the retreating side (RS) and offset the tool toward the advancing side (AS), where the harder material should be placed, in order to increase the heat input and promote a vortex-like flow that enhances the joint properties. At the same time, more pronounced heat input favours the IMCs formation and increases the thickness of the IMCs layer, especially for Al-Cu, Al-Ti and Al-Mg pairs characterized by a low melting eutectic phase. A limited IMC layer, approximately in the range of 2 – 4 μm, is instead desirable to enhance the joint strength. Variations in the process conditions of conventional FSW are suggested to deal with competitive-nature phenomena involved in the welding and thus enhance the properties in dissimilar joints. Safi et al. (2016) argued that warm FSW (WFSW) provides improved mechanical properties of Al-Cu system.~~ Indeed, preheating of copper plate allows one to obtain a more homogeneous and finer microstructure attributable to the reduced thermal gradient between the stir zone and the parent material, resulting in an increasing of tensile strength.~~ Yaduwanshi et al. (2016) experimented a plasma assisted FSW for dissimilar Al-Cu system and claimed an increase in joint efficiency.~~ The preheating of the copper side (which reach a higher temperature of approximately 300 K than the aluminum) reduces the yield stress difference between the two metals favoring the material flow from the AS to the RS and thus enhancing the material mixing in the weld bead. The authors reported an increase of even 100% of tensile strength with respect to the conventional FSW.~~ Liu et al. (2015) implemented electrically assisted FSW and tested it on dissimilar AA6061-TRIP steel 780 welding. ~~The authors observed effectiveness in material flow due to the electrical softening especially on the steel side, leading to favorable materials interlocking and also to a reduction of required welding forces.~~ Bang et al. (2012) obtained improved joint strength relative to Al base material with gas tungsten arc welding (GTAW) assisted FSW for dissimilar aluminum alloy-stainless steel pair.~~ Adopting the same concept of GTAW assisted FSW, Bang et al. (2013) and Joo (2013) reported increases in tensile strength of dissimilar titanium-AA6061-T6 and AZ31B-mild steel systems respectively~~. Similar to aforementioned dissimilar systems, Al-Mg system have been also subjected to hybrid FSW as limitedly reported. Chang et al. (2011) improved tensile strength by introducing Ni foil third material with laser assisted FSW process variation due to the less formation of IMCs for AZ31B-H24 to AA6061-T6 system observed. Ji et al. (2017a) obtained relatively thicker IMC layer promoting the creation of the joint by having stationary shoulder diameter FSW for dissimilar AZ31B to AA6061 system. Ji et al. (2017b) and Lv et al. (2018) improved the AZ31B-AA6061 joint by ultrasonic assisted FSW. Further variations in the FSW process of stationary shoulder with ultrasonic assistance were developed by Liu et al. (2018) for AZ31B-AA6061 system, wherein noted improvements in formation of IMCs and tensile properties.

Apart from conventional FSW and process variations with heating enhanced FSW, the concept of cooling submerged FSW is rudimentary reported. Mehta and Badheka (2017) drastically reduced the formation of IMCs and enhanced tensile strength with water cooling assisted FSW in case of Al-Cu structure. In case of AZ31-AA5083 system, Mofid et al.

(2012a) and Mofid et al. (2012b) suppressed the formation of IMCs with the effect of submerged FSW in underwater and under liquid nitrogen conditions respectively. Zhao et al. (2015) conducted similar concept of underwater FSW for AZ31-AA6013 system and found better tensile properties. In practice, it is very difficult to subject the workpiece to underwater or any other submerged cooling source, therefore, cooling assisted FSW (CFSW) process variation, where cooling nozzle is subjected behind FSW tool, is suggested in the present study. In this variant of the process, here applied for the first time in the dissimilar welding of aluminum to magnesium, the heating of the adjoining material is reduced due to applied cooling facility. Consequently, a relatively minor amount of IMCs is formed, leading to enhanced mechanical properties. If compared to the submerged FSW process, the CFSW process allows one to better control the heat removal from the material to be welded. Aiming to investigate the effectiveness of CFSW process, exclusive comparisons of microstructural features, IMCs formation and mechanical properties of friction stir welded Al-Mg joints obtained with and without cooling source are comprehensively presented in this investigation.

2. Materials and methods

6 mm thick AA6061 aluminum alloy and AZ31B magnesium alloy were used as base materials for dissimilar joining by FSW and CFSW in this study. Butt joint configuration was considered. Composition and properties of base materials are mentioned in Table 1 and Table 2, respectively. The used tool, in both welding processes, was realized in H13 material, with shoulder diameter of 20 mm, pin diameter of 7 mm and 1 mm pitch left hand threaded cylindrical pin profile.

Table 1 Chemical composition of the base materials

Materials	Si	Fe	Cu	Mg	Mn	Cr	Zn	Ti	Ni	Al
AA6061-T651	0.56	0.30	0.17	1.03	0.12	0.11	0.08	0.03	-	Bal.
AZ31B	0.005	0.002	0.001	Bal.	0.29	-	0.79	0.021	0.002	2.79

Table 2 Mechanical properties of base materials

Material	Tensile Strength [MPa]	Yield Strength [MPa]	Elongation [%]

AA 6061-T651	280	240	21
AZ31B	250	185	25

Friction stir welding process was performed according to the following processing conditions and parameters: 2 mm tool pin offset towards Mg side, placement of Al material in AS and Mg in RS, rotational speed, travel speed, and tilt angle set as 1070 RPM, 70 mm/min, and 3°, respectively. CFSW was conducted with additional water cooling facility, assisting the already described conventional process. The water cooling nozzle was attached behind the FSW tool as schematized in Fig. 1. The distance between tool and water cooling source and water flow rate were kept as 15 mm and 100 ml/minute respectively.

The adjoined materials were sectioned orthogonally to the welding direction to extract the specimens for microstructure analysis and microhardness measurement. A conductive thermoset resin was used to mount the specimens that, afterwards, were lapped on abrasive discs and polished on tissue discs using a polycrystalline diamond paste (0.05-9 µm). The microstructure materialized by the welding process was revealed etching the polished section using a hydrofluoric acid in water solution. Optical microscopy was carried out to appreciate the presence of eventual internal defects, then high magnification images were acquired using scanning electron microscopy (SEM), performed using a Hitachi TM3000 device. The same equipment was employed for energy dispersive X-ray spectroscopy (EDX).

The impact of microstructure modification of local mechanical properties was investigated by Vickers microhardness tests, executed according to a programmed map using a LEICA VMHT-AUTO machine. In particular, measurements were carried out along five linear and parallel patterns, separated by 1 mm each other, in the cross section of the joint, assuming the mid-thickness as reference path. The distance between two consecutive indentations, the indentation load, the loading time and indentation speed were set such as 1 mm, 100 gf (0.98 N), 15 s, and 60 µm/s respectively.

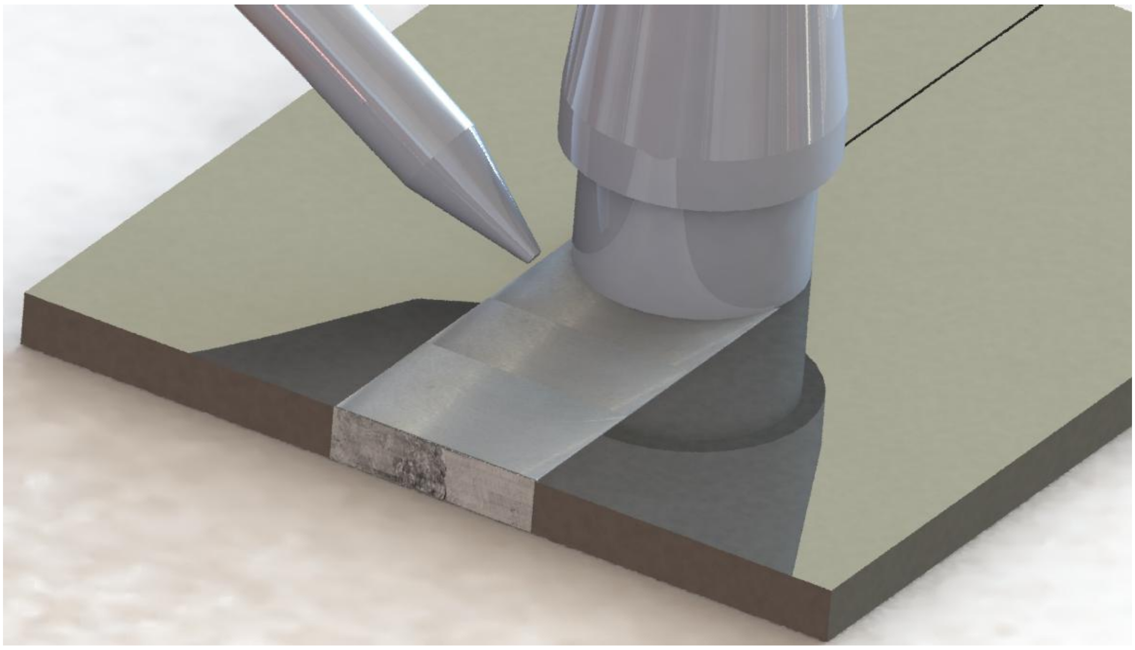

Fig. 1 – Cooling assisted friction stir welding setup

The tensile test was carried out as per the ASTM E8 standards on mini specimens of 6 mm thickness, as shown in Fig. 2. The cross head speed for the tensile test was kept as 1 mm/min. Three tensile specimens were extracted from the same weld condition coupon in order to have average values of it. Extraction of these tensile specimens was done from the middle of the specimen (Fig. 2) by wire electro discharge cutting. Ultimate tensile strength and elongation to fracture were noticed after tensile testing. Finally, X-ray diffraction analysis was performed to precisely identify the process induced IMCs.

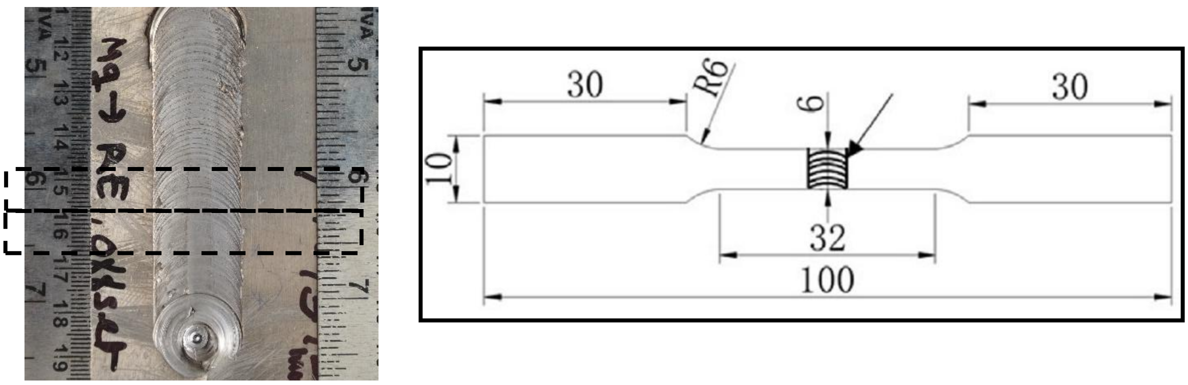

Fig. 2 – Tensile testing speciemens (ASTM E8)

3. Results and discussion

Figs. 3 (a) and (b) show the surface morphologies of Al-Mg welds produced by FSW and CFSW, respectively. Defect free surfaces are observed for both of the process conditions.

Front side of stir surface is seen with rough surface having shoulder marks in case of FSW, while smooth stir surface is obtained with CFSW. Reasonably, the surface material flow is influenced by the rapid cooling action induced by the water flow that may have restricted the capability of the material to flow, resulting in a smooth stir surface. Mehta and Badheka (2017) noted similar effects for dissimilar Cu-Al FSW system.

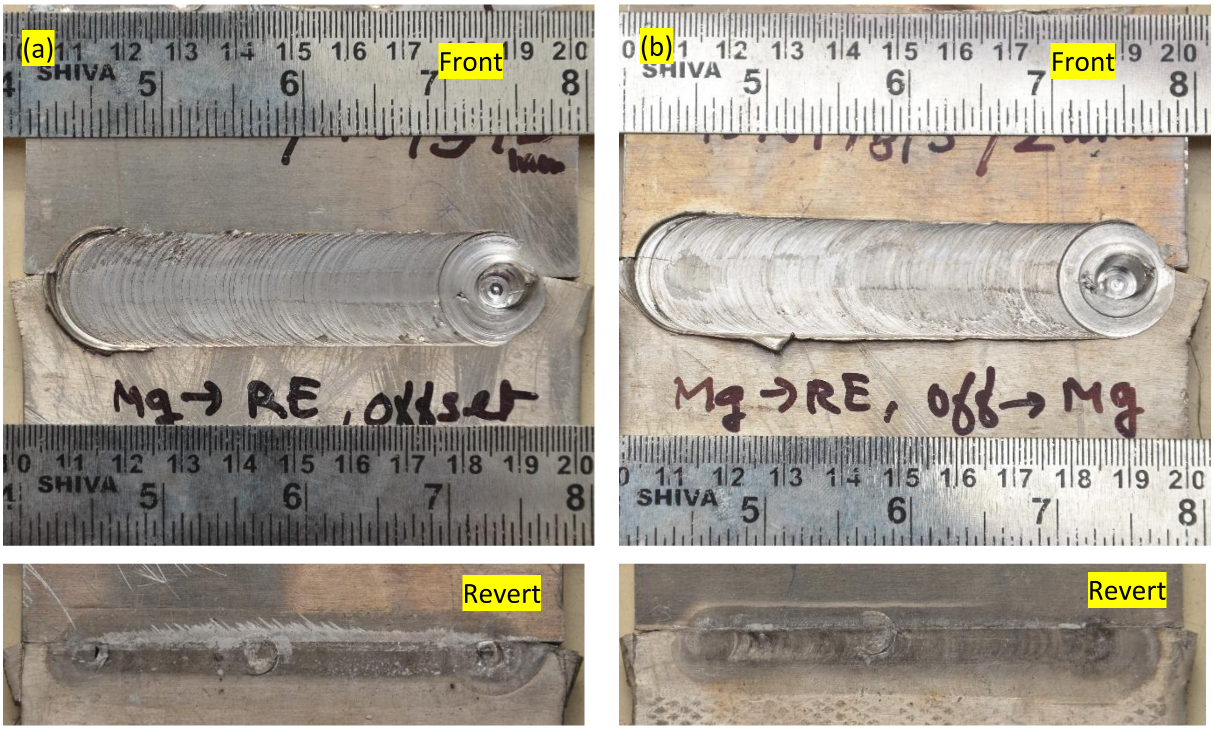

Fig. 3 – Surface morphologies (a) FSW and (b) CFSW

In Fig. 4, the macrographs of the cross sections of the two joints under investigation are reported. Both the images are built by merging more than 150 high magnification images taken in different positions in the cross section. Mishra and Mahoney (2007) mentioned four different metallurgical zones are appreciable, namely the base material (BM), the heat affected zone (HAZ), the thermo-mechanical affected zone (TMAZ), and the nugget zone (NZ). In more details, in the BM the heat input is too low to induce any microstructural variation and the parent microstructure is retained. The material in the HAZ experienced thermal cycles inducing minor changes of the microstructure (e.g. grain coarsening or a redistribution of the precipitates). In the TMAZ, the heat input, coupled with the mechanical work, produced a partially recrystallized microstructure with deformed grains. Finally a fully recrystallized microstructure with the typical onion rings is usually observed in the NZ.

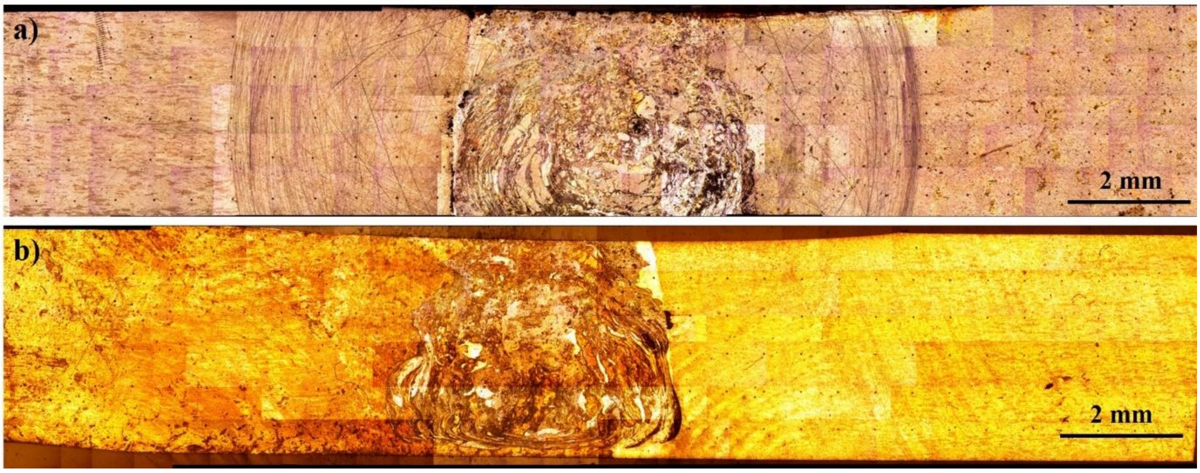

Fig. 4 – Cross section macrographs of the two joints under investigation: a) FSW; b) CFSW

In Fig. 4, the boundaries of the HAZ and TMAZ are not immediately detectable, but a clear evidence of the NZ is found. The NZ for both the joints appears very complex, due to the occurrence of a multi-material plastic flow and the formation of IMCs.

No significant defects, namely cracks or tunnel type defects, were found. The NZ exhibited a pronounced irregularly shaped region close to the weld line. The irregular shaped region has a kind of trapezoidal shape observable in the upper portion of the NZ and the weld interface near the upper surface is shifted from the initial weld centerline to the AS. It is also possible to appreciate a sharp transition between both the base materials suggesting that both alloys penetrate each other in the form of vortex and swirl like features. Zettler et al. (2006) commented similar features for Al6040-AZ31 joints. In particular, a significant mixing between the two materials was detected resulting in a complex nugget zone characterized by a trapezoidal shaped upper zone due to the dominant flow of Aluminum from the advancing side and by a bulbous region in the lower portion.

High magnification images from the different zones are provided in Fig. 5 and Fig. 6, evidencing also the location of the acquisition, aiming to better present and discuss the microstructure produced during the welding. The micrographs of the base material are also given to better discuss the microstructural changes induced.

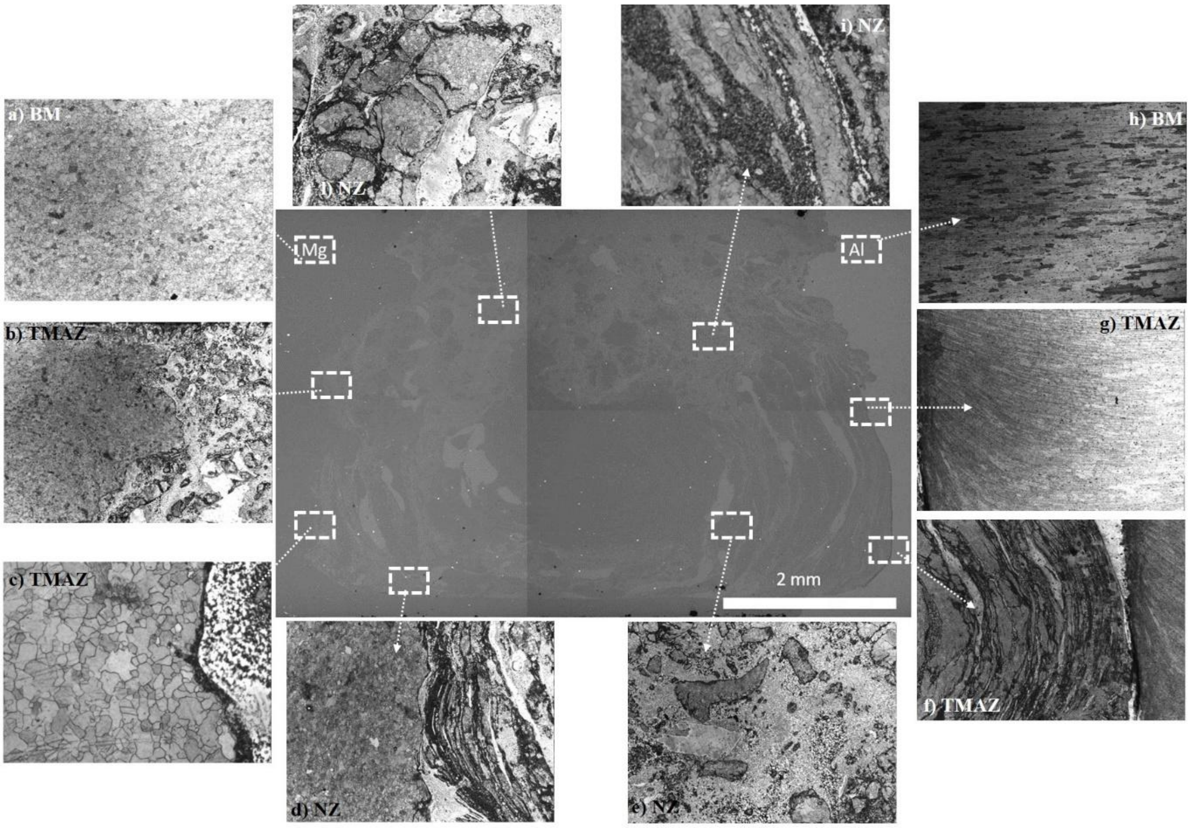

Fig. 5 – High magnification micrographs taken in the cross section of the CFSW joint: a) magnesium base material; b) magnesium side TMAZ c) magnesium side TMAZ; d) NZ; e) NZ; f) aluminum side TMAZ; g) aluminum side TMAZ; h) aluminum base material; i) NZ; l) NZ. The central SEM low magnification image highlights the locations of each acquisition.

In the aluminum BM (Fig. 5h), the pancake-like microstructure, with stretched grains along the rolling direction, is evidenced. Some second phase black particles are appreciable as well. The presence of these particles is due to the heat treatment that leaded to the formation of precipitates, i.e. the above mentioned second phase black particles. The microstructure of the BM in the magnesium side (Fig. 5a) appears as homogenous and made of equiaxed grains, with mean dimension of approximately 15 microns. The precise identification of the HAZs is very challenging; indeed, only in the aluminum an evidence of its presence is found in the slight redistribution of the precipitates. In Fig. 5g the TMAZ on the aluminum side is reported. Highly deformed and stretched grains are clearly visible, congruently with the proximity to the stirred material in the NZ. Fig. 5f highlights the boundary region between the NZ and the TMAZ - Al side. These two regions seem to be separated by a diffusion layer. Moreover, in the NZ some onion rings are visible, made of mixed structures and IMCs. The lamellar like bands rich in aluminum and magnesium were also described and discussed by Azizieh et al. (2016) in their paper studying the dissimilar FSW of AZ31 to AA 1050. The authors argued that the different thickness observed in the rings is probably due to the mismatching of the flowability of the two materials. Concerning the TMAZ magnesium side (Fig. 5b), a completely different microstructure can be observed: the grains appear undeformed and retaining the parent microstructure. The difference between the TMAZ Mg side and the TMAZ Al side was also discussed by Kostka et al. (2009) for the AA6040 and AZ31 FSW.

Looking at Figures 5d,e,i,l, (taken in the NZ), it is possible to observe presence of magnesium, probably removed by the pin from the TMAZ (Mg side) and drown inside the NZ, as a consequence of the flow continuously promoted by the rotating pin. The complex microstructure, quite different with respect to Al and Mg similar FSW, observed in the NZ well reflects the remarkable chemical affinity of Al and Mg and their inclination to form IMCs. Indeed, the NZ is mainly constituted by Al-Mg solutions within recrystallized grains, retaining also Mg pieces with the microstructure of the parent material. Besides, several phenomena affecting the microstructure, such as intercalated lamellar structure reported by Yan et al. (2005), vortex intercalated band type structure observed by Zettler et al. (2006) and equiaxed banned structure mentioned by Yan et al. (2010) can be hypothesized, as further described and discussed hereinafter on the base of SEM and XRD observations. Within the central picture, depicting the weld bead, it is possible to observe some swirls and vortices produced by the complex material flow induced by the process, as proved and explained in Malarvizhi and Balasubramanian (2012). The interfaces between the different metallurgical zones are tortuous and with some interpenetrating features (IPF). Venkateswaran and Reynolds (2012) observed and discussed these results. The authors argued that the type of the interface is dictated by the adopted welding parameters and, in particular, the interface characterized by IPF (clearly visible in Fig. 5) are promoted by high rotational speeds (usually above the 900 rpm). The slight asymmetry of the IPF can be ascribed to the offset of the pin in the retreating side.

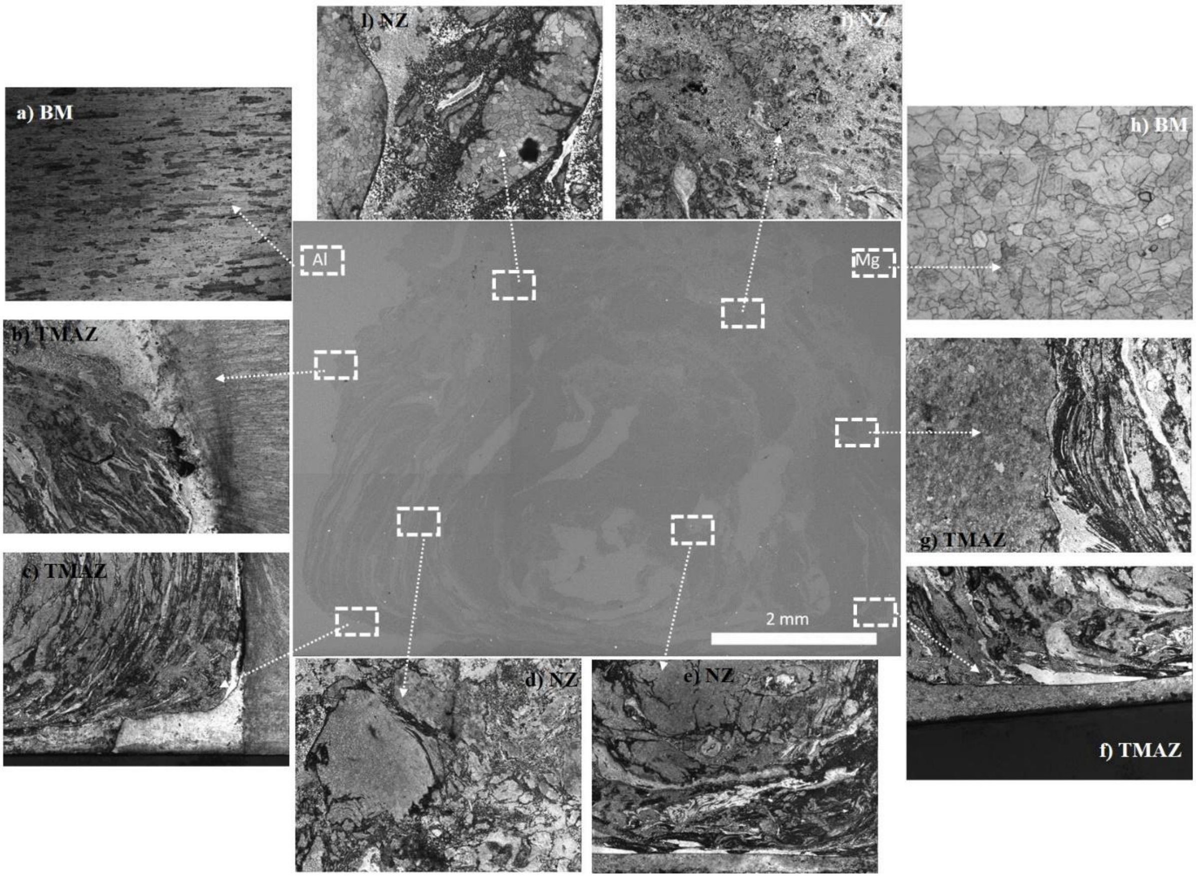

Fig. 6 – High magnification micrographs taken in the cross section of the FSW joint: a) aluminum base material; b) aluminum side TMAZ c) aluminum side TMAZ; d) NZ; e) NZ; f) magnesium side TMAZ; g) magnesium side TMAZ; h) magnesium base material; i) NZ; l) NZ. The central SEM low magnification image highlights the locations of each acquisition.

Fig. 6 reports the microstructure of the FSW joint. Qualitatively, similar observations, as already drawn for the CFSW (see Fig. 5) joint, can be pointed out, being the main significant difference given by the presence of some little cracks in the bond area between the TMAZ (Al side) and the NZ. Such cracks are clearly appreciable in Figs. 6b and 6c.

Detailed SEM observations with EDX analysis are reported below in Fig. 7 and Table 3, respectively. In particular, Fig. 7 details the interface region between the NZ and the TMAZ (Al side) as captured by high magnification SEM. EDX measurements, whose outcomes are summarized in Table 3, are carried out in the locations highlighted within the picture. As can be seen, a diffusion layer is clearly visible, identified as a solid solution of Mg in an Al matrix, between the NZ and the TMAZ (Al side).

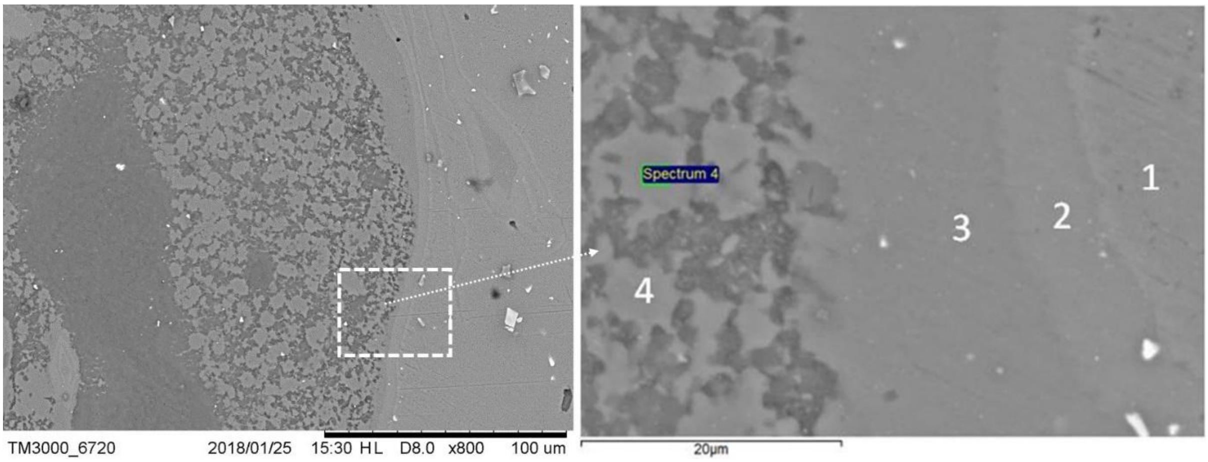

Fig. 7- SEM images of the interface between NZ and TMAZ at the Al side (CFSW joint).

Table 3 – EDX results in the locations highlighted in Fig. 7.

Zone	Chemical composition (wt %)					Interpretation	Location
	O	Mg	Al	Si	Zn		
1	3.443	13.057	83.099	0.401	-	Solid solution of Mg in Al matrix	Transition between NZ and TMAZ Al side
2	3.578	38.536	57.682	0.204	-	Phase β (Al_3Mg_2)	NZ
3	3.909	49.629	46.150	0.313	-	Phase γ ($Al_{12}Mg_{17}$)	NZ
4	4.404	55.902	39.009	-	0.684	Phase γ ($Al_{12}Mg_{17}$)	NZ

On the other hand, no diffusion layer is detected at the transition between the NZ and the TMAZ (Mg side), as shown in Fig. 8. It suggests that different phenomena occurred on the Al side and on the Mg side.

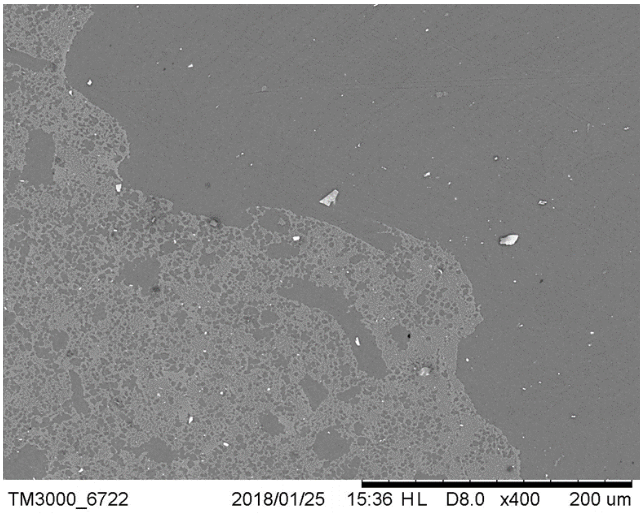

Fig. 8 –SEM images of the transition between the NZ and the TMAZ at the Mg side (CFSW joint).

The microstructure established in the NZ of the CFSW joint can be assimilated to a metal matrix composites with variable composition moving from the AS (Al side) toward the RS (Mg side). More specifically, a Mg solution in an Al matrix can be identified in the former case (Al side), while an Al solution in a Mg matrix can be observed in the other region. In both cases, IMCs are copiously distributed, as highlighted in the following images and tables, generating also an onion ring structure, confirmed by the SEM (Fig. 9) and EDX analysis (Table 4) reported below.

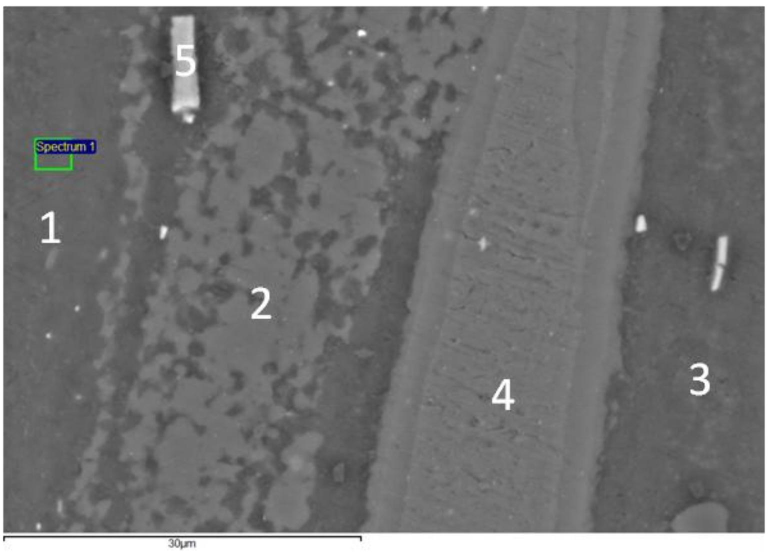

Fig. 9 – SEM images of the NZ of joint CFSW, indicating the locations of the EDX analysis.

Table 4 – EDX results in the locations highlighted in Fig. 9.

Zone	Chemical composition detected (wt %)						Interpretation
	O	Mg	Al	Si	Mn	Zn	
1	5.271	74.494	19.634	-	-	0.601	Solid solution of Al in Mg matrix
2	4.674	56.378	38.337	-	-	0.611	Phase γ ($Al_{12}Mg_{17}$)
3	7.868	72.918	18.390	0.166	-	0.657	Solid solution of Al in Mg matrix
4	4.144	15.214	80.296	0.346	-	-	Solid solution of Mg in Al matrix
5	14.800	33.687	34.205	0.355	16.953	-	$Al(Mg)_4Mn)$ IMC coming from the Mg

In case of FSW joint, the formation of IMCs and solid solution phases in the corresponding base material phases are observed, in line with what was observed in CFSW joint in terms of phase identifications, as evidenced by SEM (Fig. 10) and EDX analysis (Table 5) inside the NZ. However, the amount of IMCs formed may be different depending on the processing conditions. The volume fractions of IMCs are expected to be relatively higher in case of the joint welded by conventional FSW.

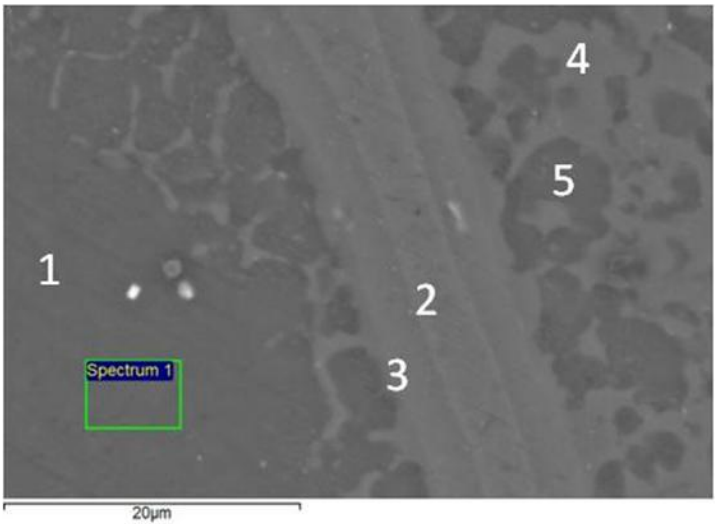

Fig. 10 – SEM images of the NZ and TMAZ (Al side) of FSW joint, highlighting the locations of the EDX analysis.

Table 5 – EDX results in the locations highlighted in Fig. 10.

Zone	Chemical composition detected (wt %)						Interpretation
	O	Mg	Al	Si	Mn	Zn	
1	4.223	86.137	8.717	-	-	0.924	Solid solution of Al in Mg matrix
2	3.712	22.520	73.505	0.264	-	-	Solid solution of Mg in Al matrix
3	3.622	50.642	45.585	0.151	-	-	Phase β (Al_3Mg_2)
4	3.767	65.130	30.456	-	-	0.647	Phase γ ($Al_{12}Mg_{17}$)
5	3.650	79.016	17.334	-	-	-	Solid solution of Al in Mg matrix

The diffractogram presented in Fig. 11, obtained from the XRD analysis of the NZ, proves that the NZ is made of Al, Mg beta phase and gamma phase. Furthermore, it univocally identifies the IMCs phases, whose presence is indicated also by the EDX investigation, as given by $Al_{12}Mg_{17}$ and Al_3Mg_2, in agreement with the analyses of Venkateswaran and Reynolds (2012) and Shi et al. (2017). The authors also observed that the presence of IMCs in the weld interface including IPF detrimentally affects the mechanical properties of the joints being a preferential path for the crack propagation during the loading of the structure. As far the IMCs phases nucleation, Kostka et al. (2009) and Fu et al. (2015) argued that such IMCs are formed because of solid state diffusion and constitutional liquation (or eutectic) mechanisms. The former occurred usually in case of low heat input during the FSW because the welding temperature usually remains below the eutectic temperatures of the Al-Mg binary phases (i.e. 437°C in the Mg dominant side and 450°C in the Al side) and thus the compounds nucleated and grew by means atoms diffusion between aluminum and magnesium. On the other hand, the authors indicated the constitutional liquation as the main factor in the formation of IMCs. Indeed, the heat generated by the friction between materials and tool during the stirring action and the material plastic deformation allows the weld zone to reach the eutectic lines. Therefore, local melting can occur forming a liquid film along the grain boundary allowing a more rapid diffusion of Al and Mg atoms and the subsequent rapid solidification produce the observed microstructure according the eutectic reactions:

$$Al\ (450°\mathrm{C}): L \rightarrow Al_3Mg_2$$

$$Mg\ (437℃): L \rightarrow Al_{12}Mg_{17}$$

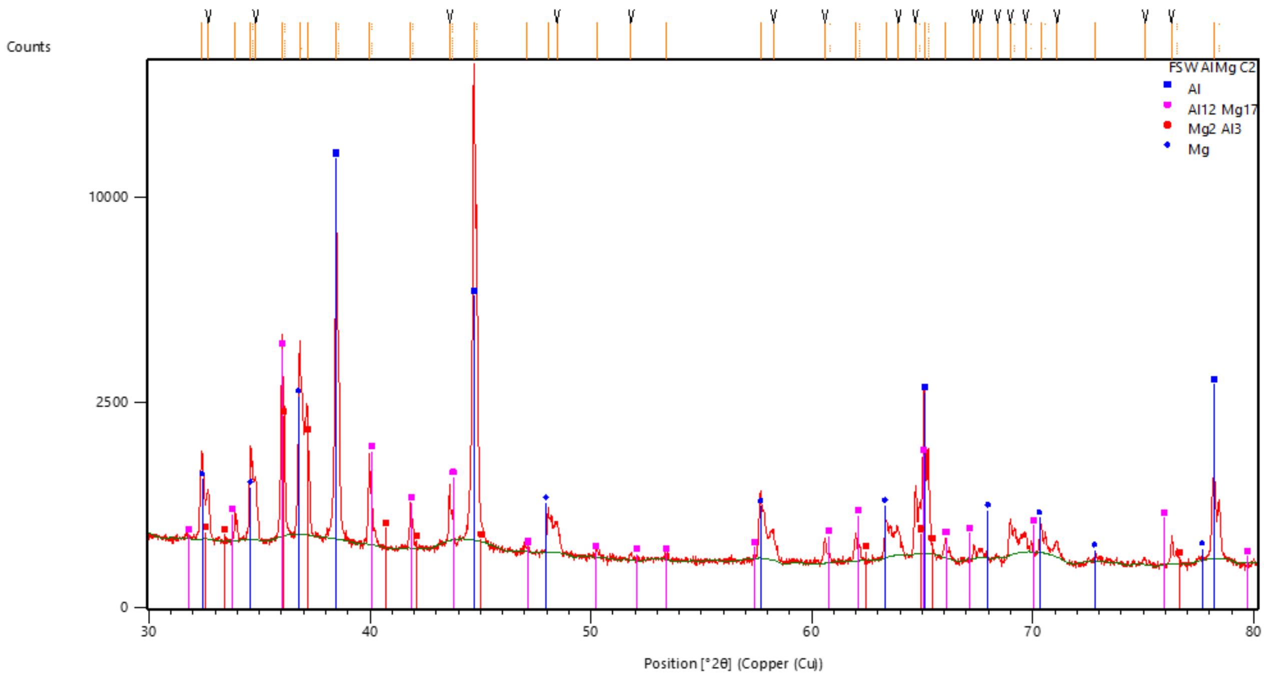

Fig. 11 – Diffractogram obtained in the NZ of the CFSW joint. Identical results were obtained in the case of standard FSW, so this image can be assumed as representative of both processing conditions.

The tensile strength and elongation measurements are presented in Fig. 12. Tensile strength of 128 MPa and 182 MPa are obtained for Al-Mg welds produced by FSW and CFSW respectively. The reason for the lower tensile strength of FSW joint is attributable to the formation of some cracks at the interface between NZ and TMAZ (Fig. 16). Similar cracks are not noticed in CFSW joint. Mofid et al. (2012b) mentioned that brittle form of IMCs is a major reason for the crack, because the fracture preferentially propagated along the brittle intermetallic layers, as confirmed by the cleavage-type fracture surfaces observed. On the other hand, in the same work the authors claimed that underwater friction stir welding presents a ductile fracture surface, pointing out a reduced amount of IMCs formed during the weld. There are no defects reported in the detailed analysis of microstructure examinations of CFSW. The amount of IMCs in case of FSW joint is less than the CFSW joint, based on studies by Mofid et al. (2012b) and Mofid et al. (2012a). Therefore, improvement in tensile strength is achieved with the CFSW relative to FSW.

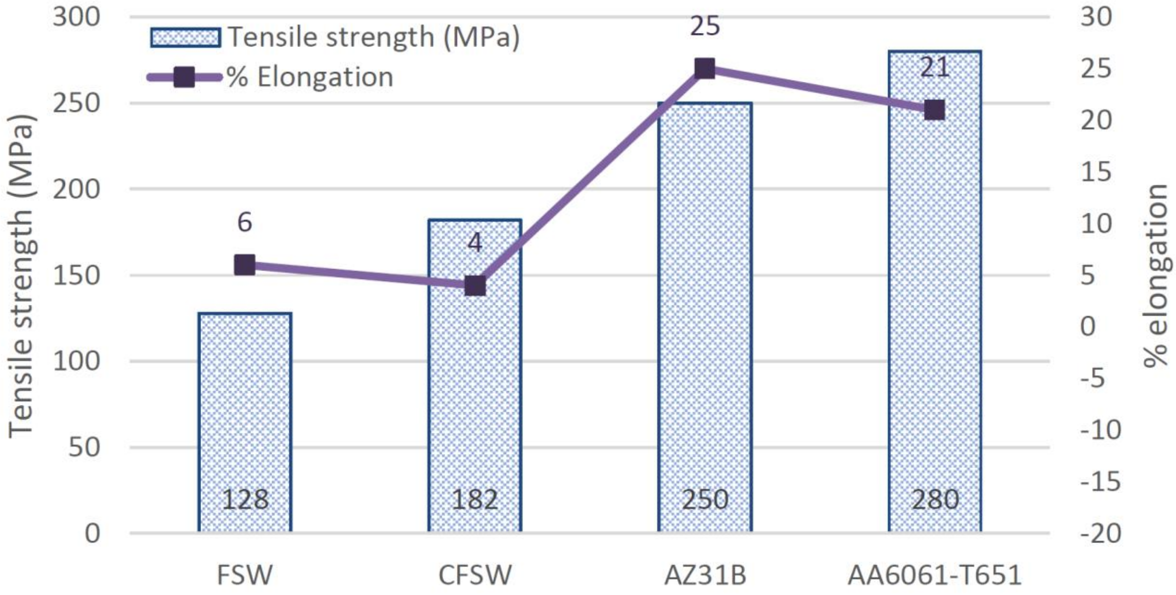

Fig. 12 – Tensile properties of welds and base materials and images of the broken specimens.

Low percentage of elongation is reported for both of the welds of FSW and CFSW, if compared to the base materials. Large amount of IMCs, precipitates and different phases, identified in above analysis, are responsible for the low percentage of elongation of both the joints. Shi et al. (2017) demonstrated that the mechanical properties of the joints are ruled by the IMCs and the chemical composition, size and distribution of the above mentioned IMCs are in turn regulated by the processing conditions. The CFSW failed on the boundary of the weld bead: both the specimens showed a fragile fracture, suggested also by the low values of the elongation measured. Concerning the tensile tests carried out on the parent materials, a typical ductile fracture with necking occurrence was observed.

The ultimate tensile strength (UTS) values measured for the CFSW joints are close to the 73% to the ones of the AZ31B base material; to make a comparison Fu et al. (2015) in their work on the FSW of AA 6061 and AZ31 obtained an UTS close to the 70% of the Mg parent material and Yan et al. (2005) in their paper studying the FSW of AA 1060 and AZ31 obtained a joint with an UTS close to the 67% of the Al one. The samples showed a brittle fracture probably induced by the fragile IMCs. Dorbane et al. (2016) provided similar results, reporting that the conventional FS welded joints exhibit a very low joint efficiency (evaluated as the ratio of the UTS of the Al-Mg welded samples and the UTS of parental weaker parental material) between 18% and 55% depending the process parameters.

Photographs of the tested specimens, one for each sample (namely FSW, CFSW, Al parent material and Mg base material), are given in figure 13. As appreciable, both the CFSW and FSW samples failed on the Al side of the joint while the Al base material, as expected, showed a more ductile behavior. Concerning the welded sample, the failure location was observed in the middle of the Al-Mg mixed area for FSW samples, while the CFSW samples failed on the boundary of this region on the aluminum side.

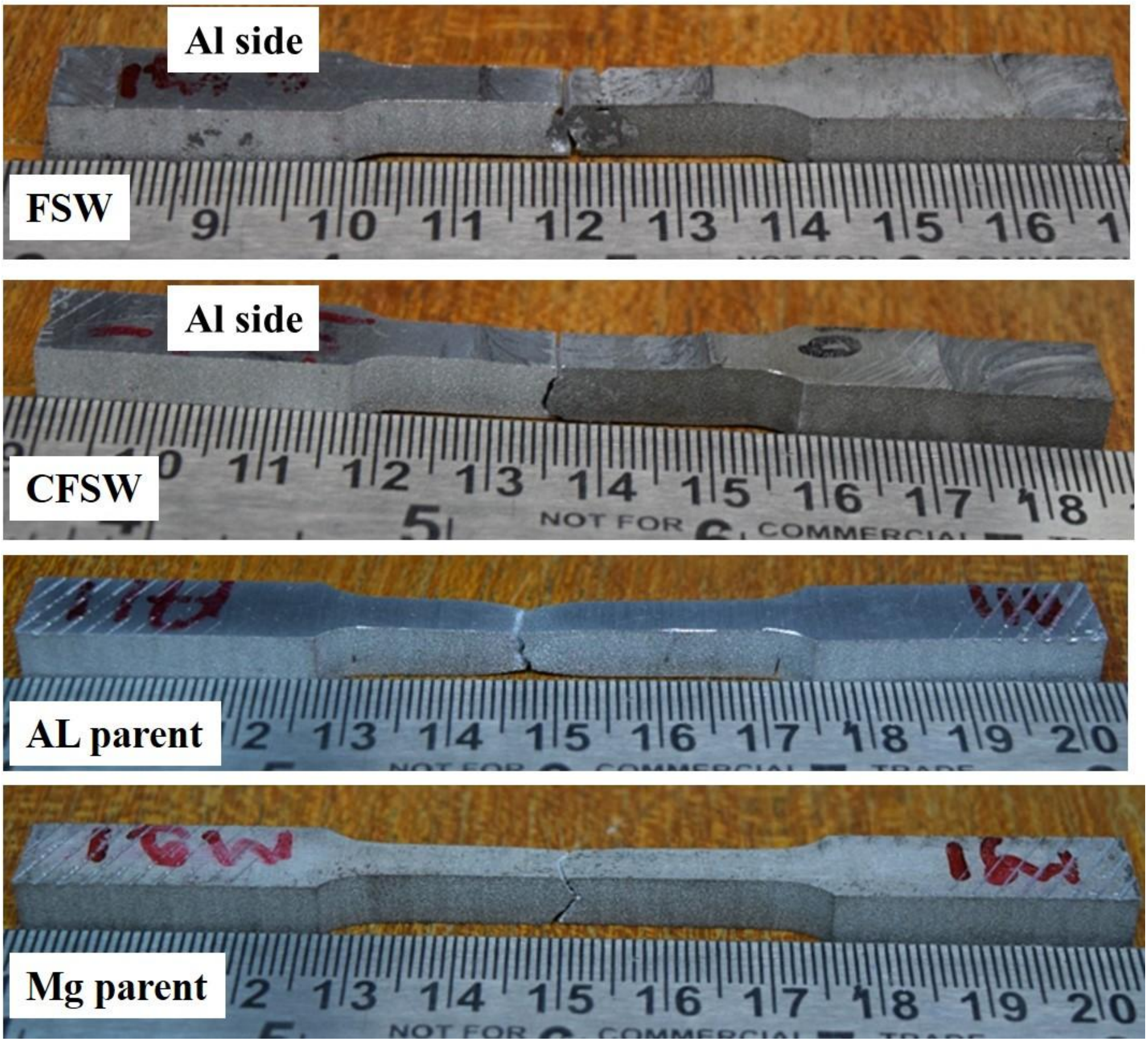

Fig. 13 – Photographs of the tested specimens, one for each sample tested.

High magnification SEM micrographs of the fracture surfaces for the FSW and CFSW specimens are showed, respectively, in figures 14 and 15.

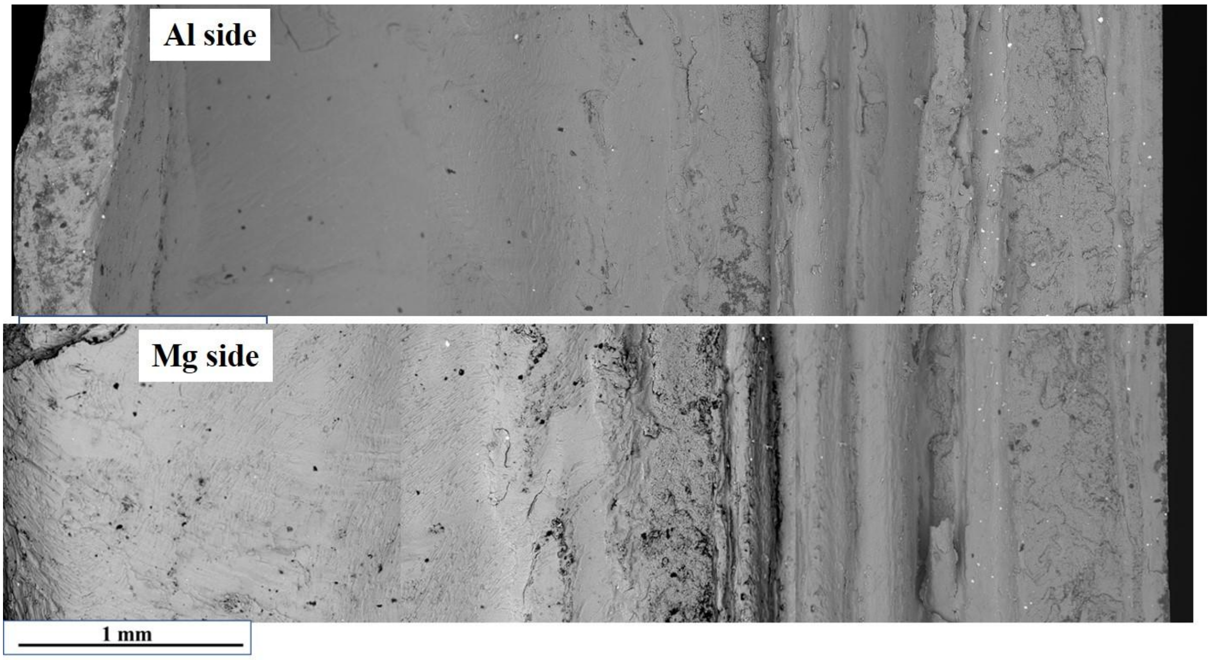

Fig. 14 – High magnification SEM micrographs of the fracture surfaces of the FSW joint.

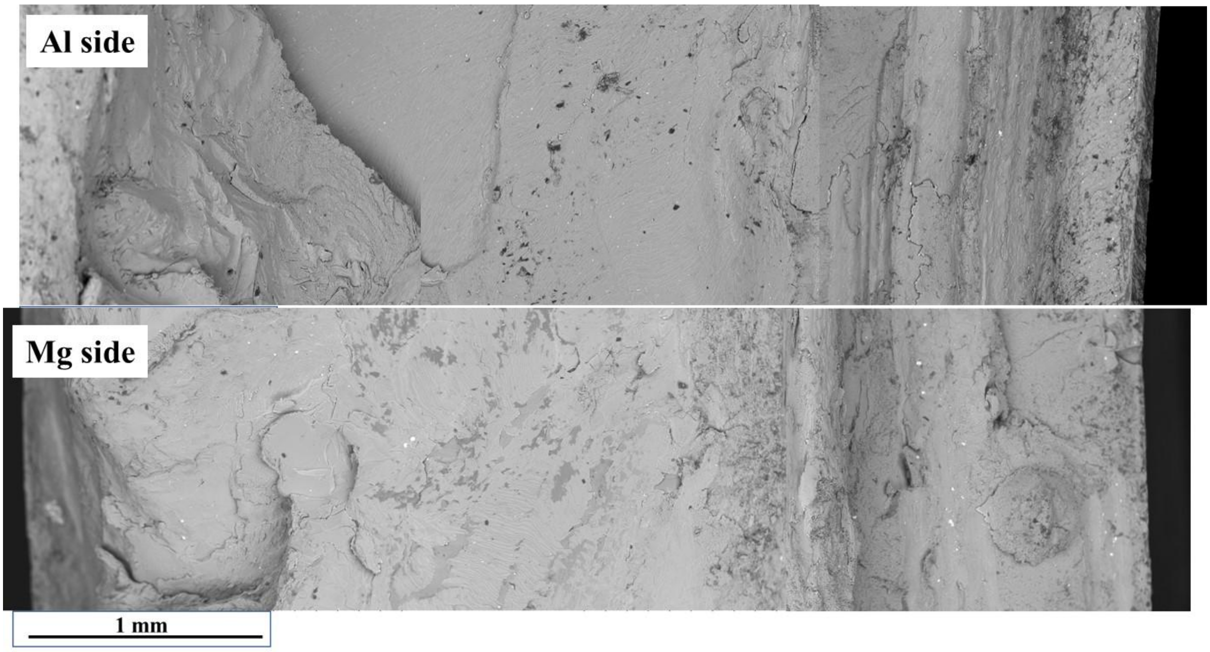

Fig. 15 – High magnification SEM micrographs of the fracture surfaces of the CFSW joint.

The SEM analysis of the failure surfaces highlighted some differences in the rupture mode between the differently welded joints, whereas the FSW samples exhibited a prevalently brittle failure mode due to the higher amount of IMCs.

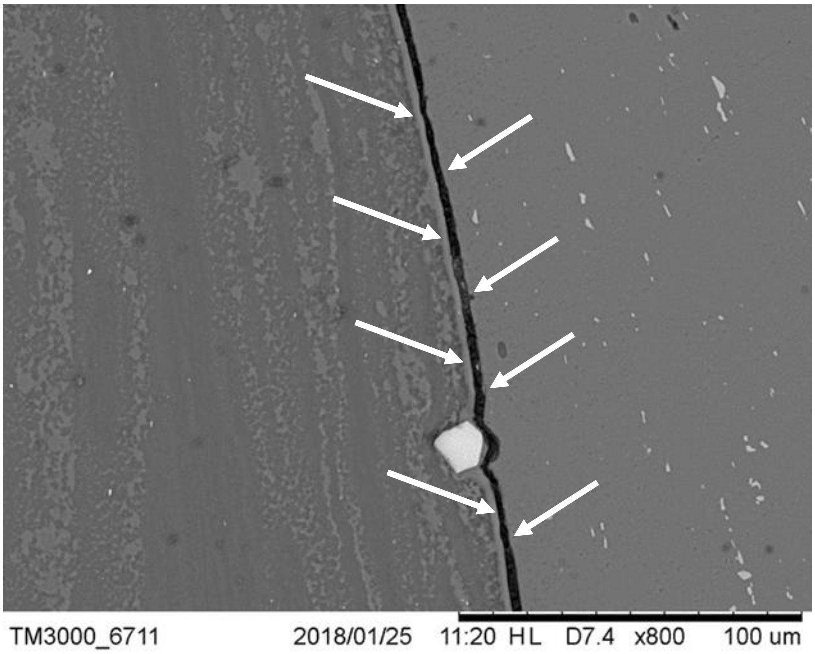

Fig. 16 – High magnification SEM micrograph of a crack between the NZ and the TMAZ Al side (FSW joint).

Fig. 17 and Fig. 18 present the micro hardness distribution measured in FSW and CFSW joints, respectively. NZ consists of very high hardness compare to Al and Mg base materials in both the process conditions. The high values observed are mainly due to the presence of IMCs in the NZ. Highest peak of 298 HV is reported for CFSW joint in the NZ (Fig. 18). The maximum peak of hardness in case of FSW joint is 204 HV (Fig. 17). This shows the presence of IMC only at that particular location, which has resulted into such high hardness values. It confirms that amount of IMCs formed are maximum in case of FSW joint compared to the CFSW joint. The cooling effect may have reduced the amount of IMCs. Mofid et al. (2012a) and Mehta and Badheka (2017) reported similar results of IMCs by having additional cooling effects in FSW. The authors observed a hardness values in the stir zone not much higher than the parental metals pointing out a reduced formation of IMCs in the cooled assisted FSW w.r.t. the conventional FSW.

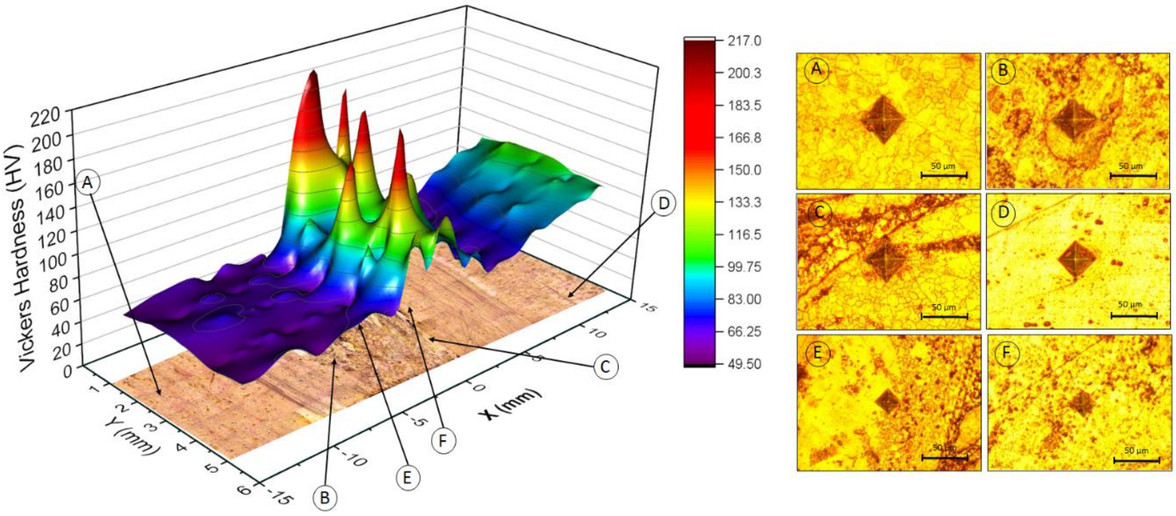

Fig. 17 - Microhardness distribution for FSW joint, including some representative indentations (A: Mg base material – HV 64.8; B, C: nugget zone – HV 69.9, 89.5; D: Al base material – HV 95.7; E, F: IMCs in the nugget zone – HV 199, 204)

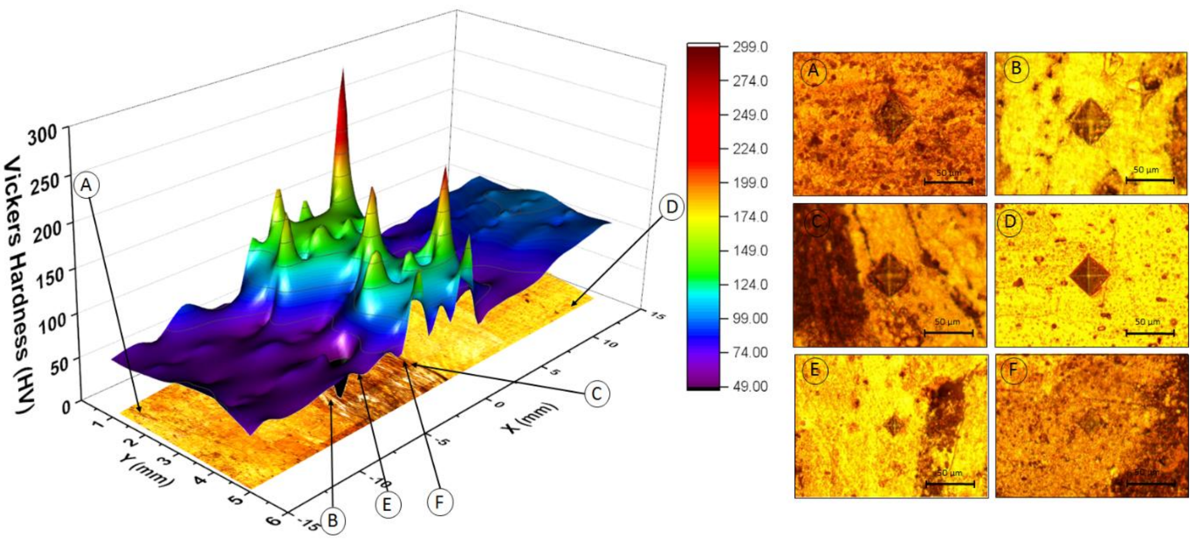

Fig. 18 - Microhardness distribution for CFSW joint, including some representative indentations (A: Mg base material – HV 66.1; B, C: nugget zone – HV 138, 77.6; D: Al base material – HV 93.8; E, F: IMCs in the nugget zone – HV 298,159)

4. Conclusions

- The mechanical properties, namely tensile strength and micro hardness of dissimilar Al-Mg joints are enhanced by CFSW relative to FSW joints. The tensile strength of 182 MPa is reported for CFSW joint while 128 MPa is reported for FSW joint.

- The CFSW presents a higher joint efficiency of approximately 73%, than the conventional FSW, which provides a value of 51%, that is in agreement with the values commented in the dedicate literature, proving the effectiveness of the suggested method.
- NZ is reported with onion rings composed of phases such as Mg in an Al matrix, Al in an Mg matrix, Al_3Mg_2, and $Al_{12}Mg_{17}$.
- A diffusion layer, identified as a solid solution of Mg in an Al matrix, was observed between the NZ and the TMAZ at the Al side, while no diffusion layer was detected between NZ and TMAZ at the Mg side.
- Maximum hardness peaks are reported in the NZ of FSW joint relative to CFSW joint. Higher average hardness values were measured in the NZ of the FSW joint suggesting the formation of a significant amount of IMCs. Cooling assisted friction stir weld is characterized by lower hardness. Isolated highest peaks can be observed only at specific locations.

Acknowledgements

The authors would like to thank the Institute of Engineers, India for providing funding (Project ID : RDUG2017010) for the present investigations.

Data availability statement

The authors declare that the raw data required to reproduce these findings are available to download from [INSERT PERMANENT WEB LINK(s)]. The processed data required to reproduce these findings are available to download from [INSERT PERMANENT WEB LINK(s)].

References

Atabaki, M.M., Nikodinovski, M., Chenier, P., Ma, J., Harooni, M., Kovacevic, R., 2014. Welding of Aluminum Alloys to Steels: An Overview. J. Manuf. Sci. Prod. 14, 59–78. https://doi.org/10.1515/jmsp-2014-0007

Azizieh, M., Sadeghi Alavijeh, A., Abbasi, M., Balak, Z., Kim, H.S., 2016. Mechanical properties and microstructural evaluation of AA1100 to AZ31 dissimilar friction stir welds. Mater. Chem. Phys. 170, 251–260.

https://doi.org/10.1016/j.matchemphys.2015.12.046

Bang, H., Bang, H., Jeon, G., Oh, I., Ro, C., 2012. Gas tungsten arc welding assisted hybrid friction stir welding of dissimilar materials Al6061-T6 aluminum alloy and STS304 stainless steel. Mater. Des. 37, 48–55. https://doi.org/10.1016/j.matdes.2011.12.018

Bang, H., Bang, H., Song, H., Joo, S., 2013. Joint properties of dissimilar Al6061-T6 aluminum alloy/Ti–6%Al–4%V titanium alloy by gas tungsten arc welding assisted hybrid friction stir welding. Mater. Des. 51, 544–551. https://doi.org/10.1016/j.matdes.2013.04.057

Chang, W.-S., Rajesh, S.R., Chun, C.-K., Kim, H.-J., 2011. Microstructure and Mechanical Properties of Hybrid Laser-Friction Stir Welding between AA6061-T6 Al Alloy and AZ31 Mg Alloy. J. Mater. Sci. Technol. 27, 199–204. https://doi.org/10.1016/S1005-0302(11)60049-2

DebRoy, T., Bhadeshia, H.K.D.H., 2010. Friction stir welding of dissimilar alloys – a perspective. Sci. Technol. Weld. Join. 15, 266–270. https://doi.org/10.1179/174329310X12726496072400

Dorbane, A., Mansoor, B., Ayoub, G., Shunmugasamy, V.C., Imad, A., 2016. Mechanical, microstructural and fracture properties of dissimilar welds produced by friction stir welding of AZ31B and Al6061. Mater. Sci. Eng. A 651, 720–733. https://doi.org/10.1016/j.msea.2015.11.019

Fu, B., Qin, G., Li, F., Meng, X., Zhang, J., Wu, C., 2015. Friction stir welding process of dissimilar metals of 6061-T6 aluminum alloy to AZ31B magnesium alloy. J. Mater. Process. Technol. 218, 38–47. https://doi.org/10.1016/j.jmatprotec.2014.11.039

Ji, S., Huang, R., Meng, X., Zhang, L., Huang, Y., 2017a. Enhancing Friction Stir Weldability of 6061-T6 Al and AZ31B Mg Alloys Assisted by External Non-rotational Shoulder. J. Mater. Eng. Perform. 26, 2359–2367. https://doi.org/10.1007/s11665-017-2640-8

Ji, S., Meng, X., Liu, Z., Huang, R., Li, Z., 2017b. Dissimilar friction stir welding of 6061 aluminum alloy and AZ31 magnesium alloy assisted with ultrasonic. Mater. Lett. 201, 173–176. https://doi.org/10.1016/j.matlet.2017.05.011

Joo, S., 2013. Joining of dissimilar AZ31B magnesium alloy and SS400 mild steel by hybrid gas tungsten arc friction stir welding. Met. Mater. Int. 19, 1251–1257. https://doi.org/10.1007/s12540-013-6016-9

Kostka, A., Coelho, R.S., dos Santos, J., Pyzalla, A.R., 2009. Microstructure of friction stir welding of aluminium alloy to magnesium alloy. Scr. Mater. 60, 953–956. https://doi.org/10.1016/j.scriptamat.2009.02.020

Liu, X., Lan, S., Ni, J., 2015. Electrically assisted friction stir welding for joining Al 6061 to TRIP 780 steel. J. Mater. Process. Technol. 219, 112–123. https://doi.org/10.1016/j.jmatprotec.2014.12.002

Liu, Z., Meng, X., Ji, S., Li, Z., Wang, L., 2018. Improving tensile properties of Al/Mg joint by smashing intermetallic compounds via ultrasonic-assisted stationary shoulder friction stir welding. J. Manuf. Process. 31, 552–559. https://doi.org/10.1016/j.jmapro.2017.12.022

Lv, X., Wu, C., Yang, C., Padhy, G.K., 2018. Weld microstructure and mechanical properties in ultrasonic enhanced friction stir welding of Al alloy to Mg alloy. J. Mater. Process. Technol. 254, 145–157. https://doi.org/10.1016/j.jmatprotec.2017.11.031

Malarvizhi, S., Balasubramanian, V., 2012. Influences of tool shoulder diameter to plate thickness ratio (D/T) on stir zone formation and tensile properties of friction stir welded dissimilar joints of AA6061 aluminum–AZ31B magnesium alloys. Mater. Des. 40, 453–460. https://doi.org/10.1016/j.matdes.2012.04.008

Mehta, K.P., Badheka, V.J., 2017. Hybrid approaches of assisted heating and cooling for friction stir welding of copper to aluminum joints. J. Mater. Process. Technol. 239, 336–345. https://doi.org/10.1016/j.jmatprotec.2016.08.037

Mishra, R.S., Mahoney, M.W., 2007. Friction Stir Welding and Processing, 1 edition. ed. ASM International.

Mofid, M.A., Abdollah-Zadeh, A., Ghaini, F.M., Gür, C.H., 2012a. Submerged friction-stir welding (SFSW) underwater and under liquid nitrogen: An improved method to join Al alloys to Mg alloys. Metall. Mater. Trans. A Phys. Metall. Mater. Sci. 43, 5106–5114. https://doi.org/10.1007/s11661-012-1314-2

Mofid, M.A., Abdollah-zadeh, A., Malek Ghaini, F., 2012b. The effect of water cooling during dissimilar friction stir welding of Al alloy to Mg alloy. Mater. Des. 36, 161–167.

https://doi.org/10.1016/j.matdes.2011.11.004

Safi, S.V., Amirabadi, H., Besharati Givi, M.K., Safi, S.M., 2016. The effect of preheating on mechanical properties of friction stir welded dissimilar joints of pure copper and AA7075 aluminum alloy sheets. Int. J. Adv. Manuf. Technol. 84, 2401–2411. https://doi.org/10.1007/s00170-015-7877-5

Shah, L.H., Ishak, M., 2014. Review of Research Progress on Aluminum–Steel Dissimilar Welding. Mater. Manuf. Process. 29, 928–933. https://doi.org/10.1080/10426914.2014.880461

Shah, L.H., Othman, N.H., Gerlich, A., 2018. Review of research progress on aluminium–magnesium dissimilar friction stir welding. Sci. Technol. Weld. Join. 23, 256–270. https://doi.org/10.1080/13621718.2017.1370193

Shi, H., Chen, K., Liang, Z., Dong, F., Yu, T., Dong, X., Zhang, L., Shan, A., 2017. Intermetallic Compounds in the Banded Structure and Their Effect on Mechanical Properties of Al/Mg Dissimilar Friction Stir Welding Joints. J. Mater. Sci. Technol. 33, 359–366. https://doi.org/10.1016/j.jmst.2016.05.006

Simar, A., Avettand-Fènoël, M.N., 2017. State of the art about dissimilar metal friction stir welding. Sci. Technol. Weld. Join. 22, 389–403. https://doi.org/10.1080/13621718.2016.1251712

Venkateswaran, P., Reynolds, A.P., 2012. Factors affecting the properties of Friction Stir Welds between aluminum and magnesium alloys. Mater. Sci. Eng. A 545, 26–37. https://doi.org/10.1016/j.msea.2012.02.069

Yaduwanshi, D.K., Bag, S., Pal, S., 2016. Numerical modeling and experimental investigation on plasma-assisted hybrid friction stir welding of dissimilar materials. Mater. Des. 92, 166–183. https://doi.org/10.1016/j.matdes.2015.12.039

Yan, J., Xu, Z., Li, Z., Li, L., Yang, S., 2005. Microstructure characteristics and performance of dissimilar welds between magnesium alloy and aluminum formed by friction stirring. Scr. Mater. 53, 585–589. https://doi.org/10.1016/j.scriptamat.2005.04.022

Yan, Y., Zhang, D.T., Qiu, C., Zhang, W., 2010. Dissimilar friction stir welding between 5052 aluminum alloy and AZ31 magnesium alloy. Trans. Nonferrous Met. Soc. China (English Ed. 20, 2–6. https://doi.org/10.1016/S1003-6326(10)60550-X

Zettler, R., Da Silva, A.A.M., Rodrigues, S., Blanco, A., Dos Santos, J.F., 2006. Dissimilar Al to Mg alloy friction stir welds. Adv. Eng. Mater. 8, 415–421. https://doi.org/10.1002/adem.200600030

Zhao, Y., Lu, Z., Yan, K., Huang, L., 2015. Microstructural characterizations and mechanical properties in underwater friction stir welding of aluminum and magnesium dissimilar alloys. Mater. Des. 65, 675–681. https://doi.org/10.1016/j.matdes.2014.09.046

Figure 1
Click here to download high resolution image

Figure 2

Click here to download high resolution image

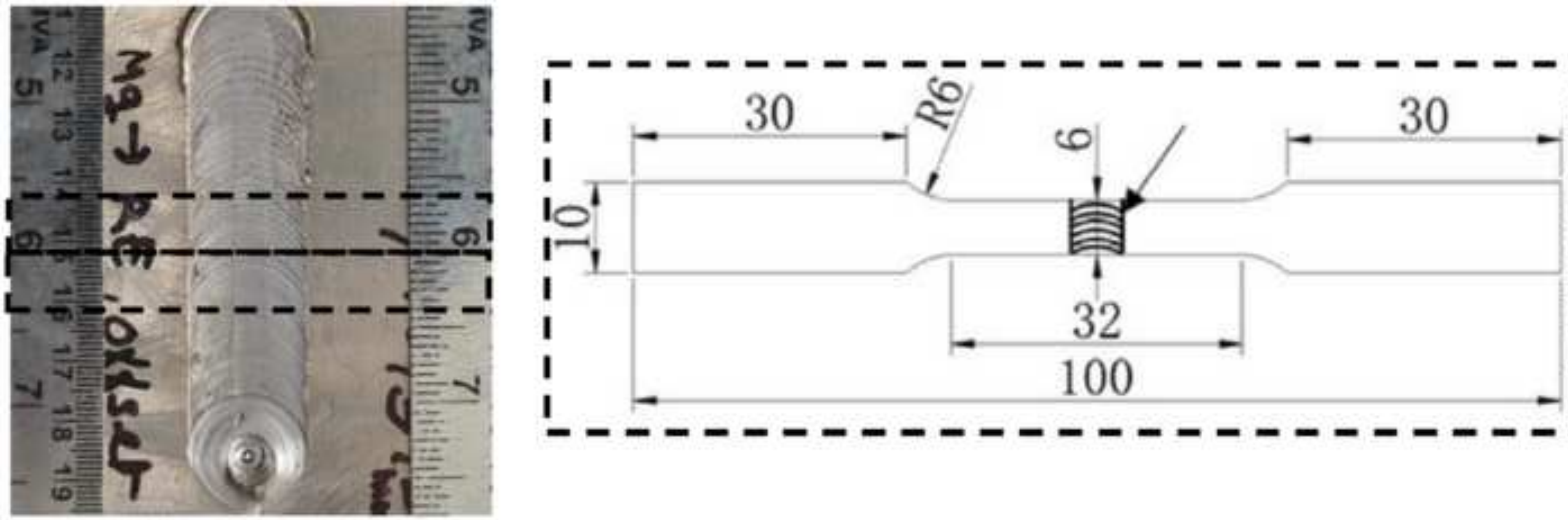

Figure 3

Click here to download high resolution image

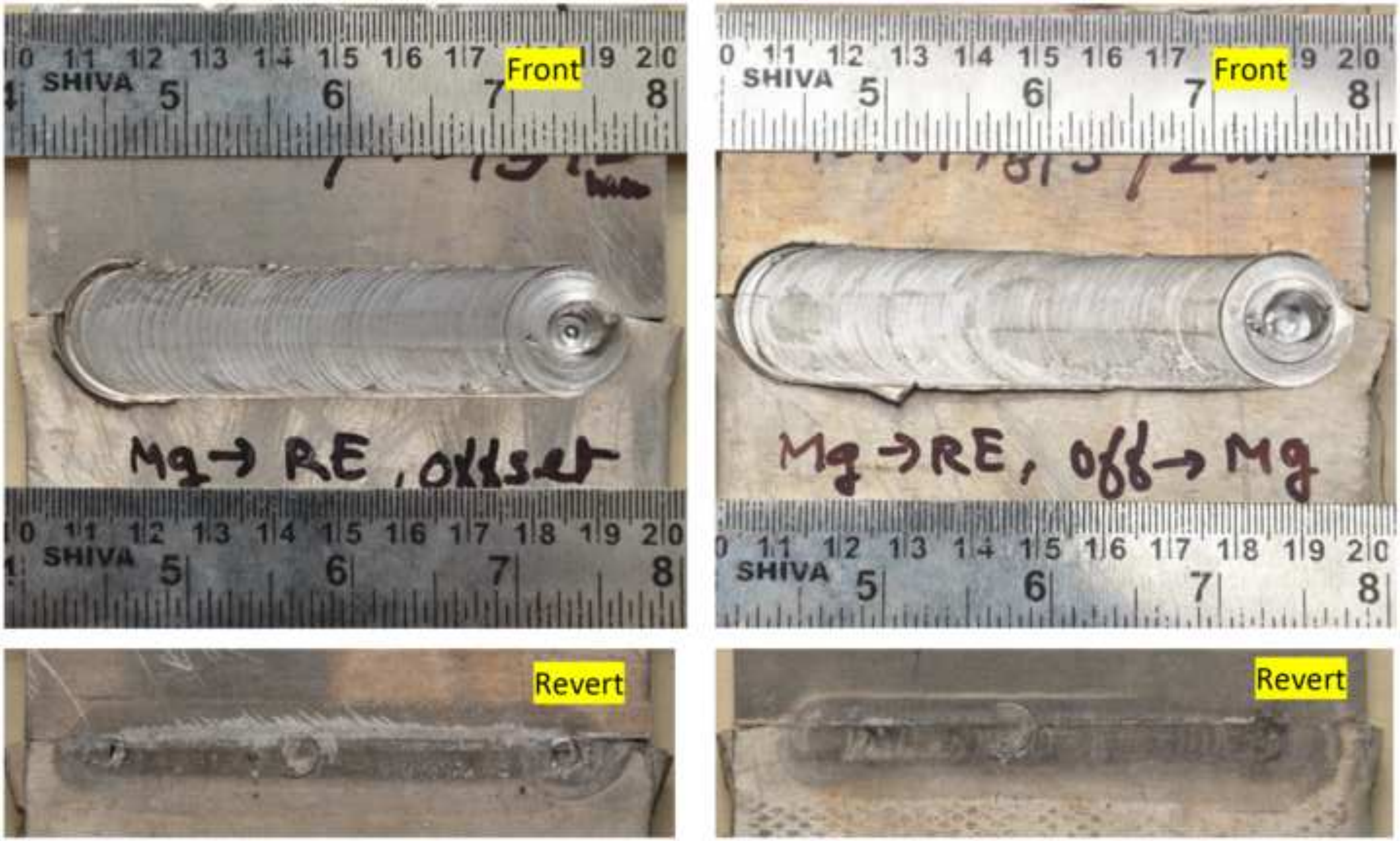

Figure 4
Click here to download high resolution image

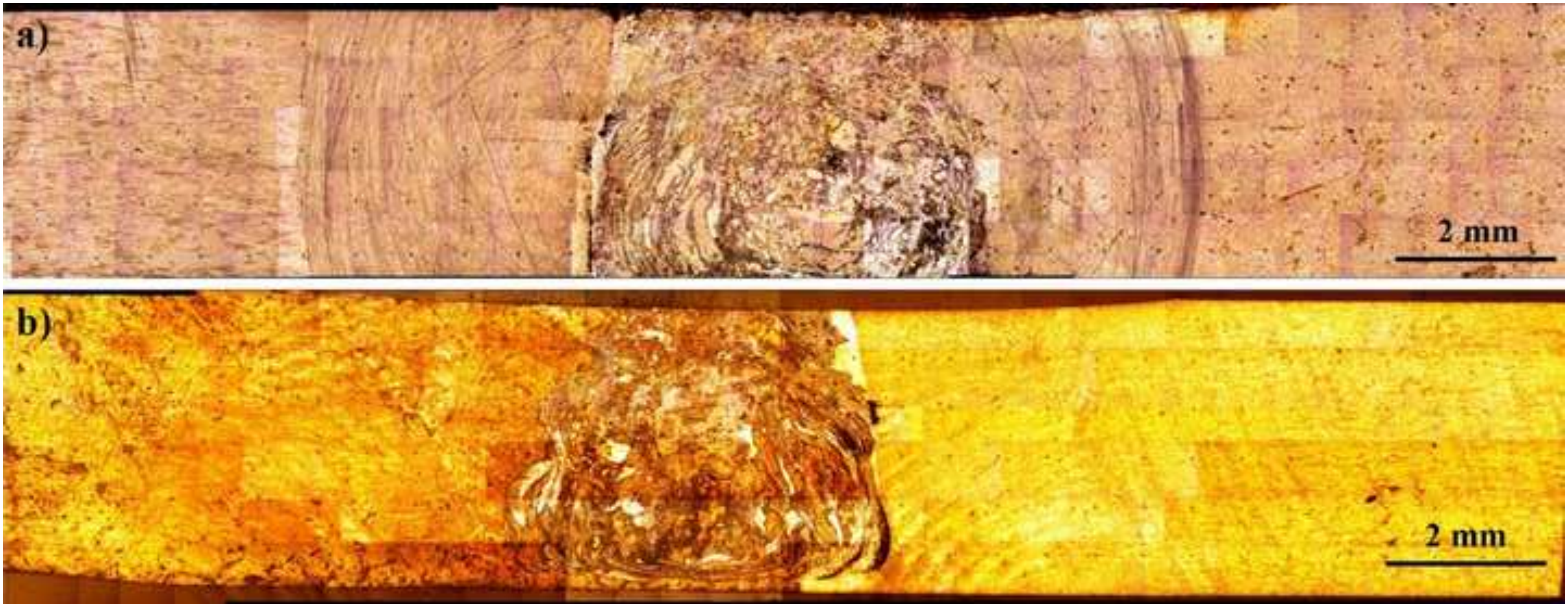

Figure 5
Click here to download high resolution image

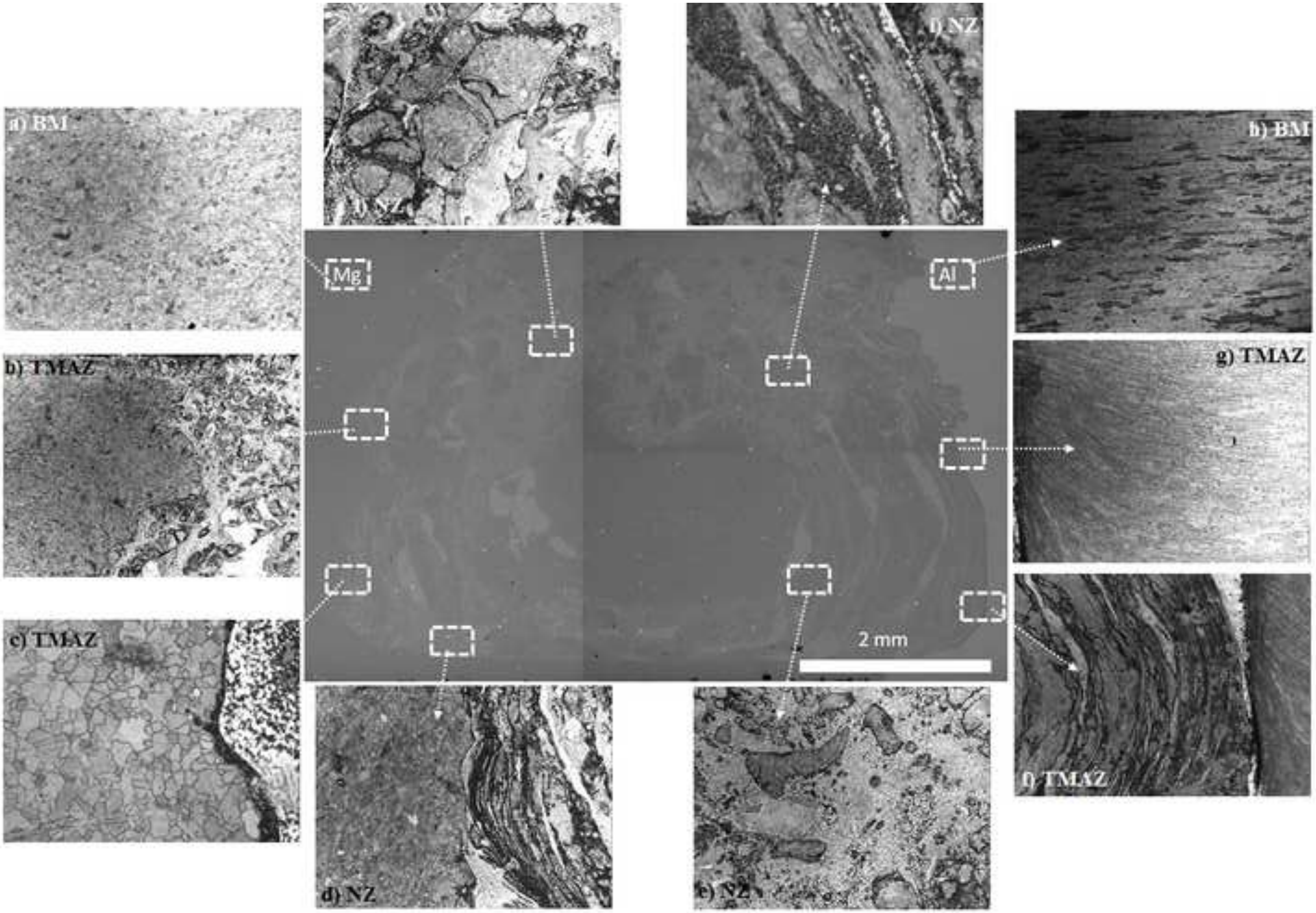

Figure 6

Click here to download high resolution image

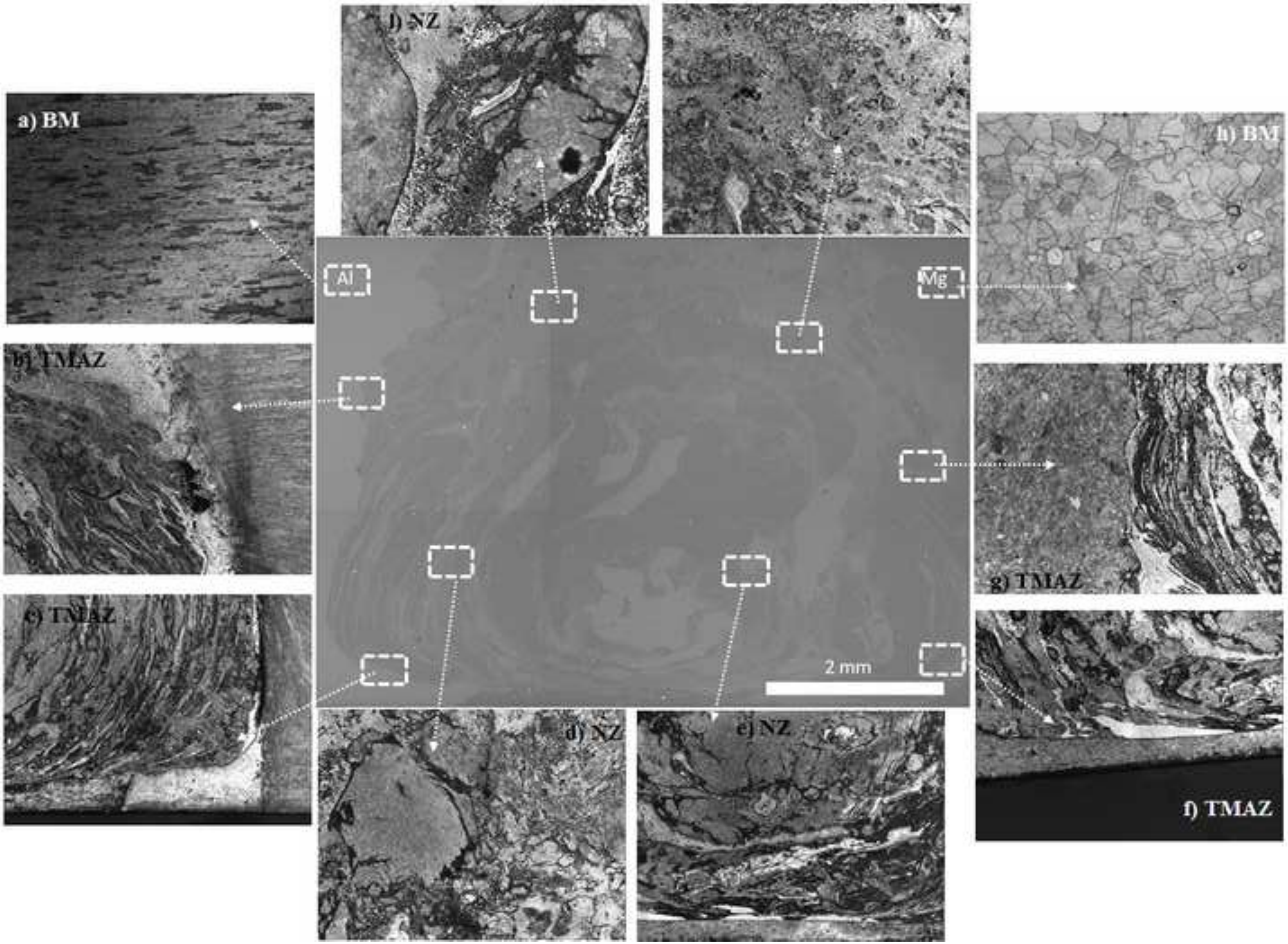

Figure 7
Click here to download high resolution image

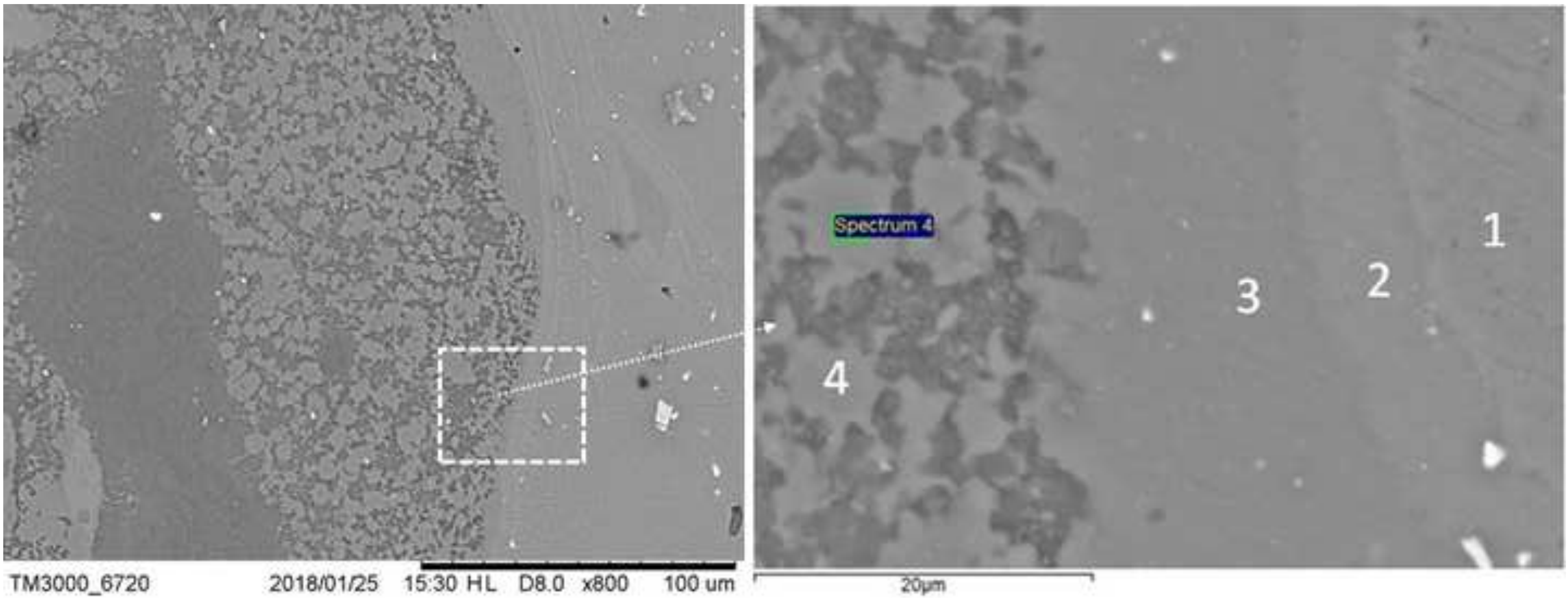

Figure 8
Click here to download high resolution image

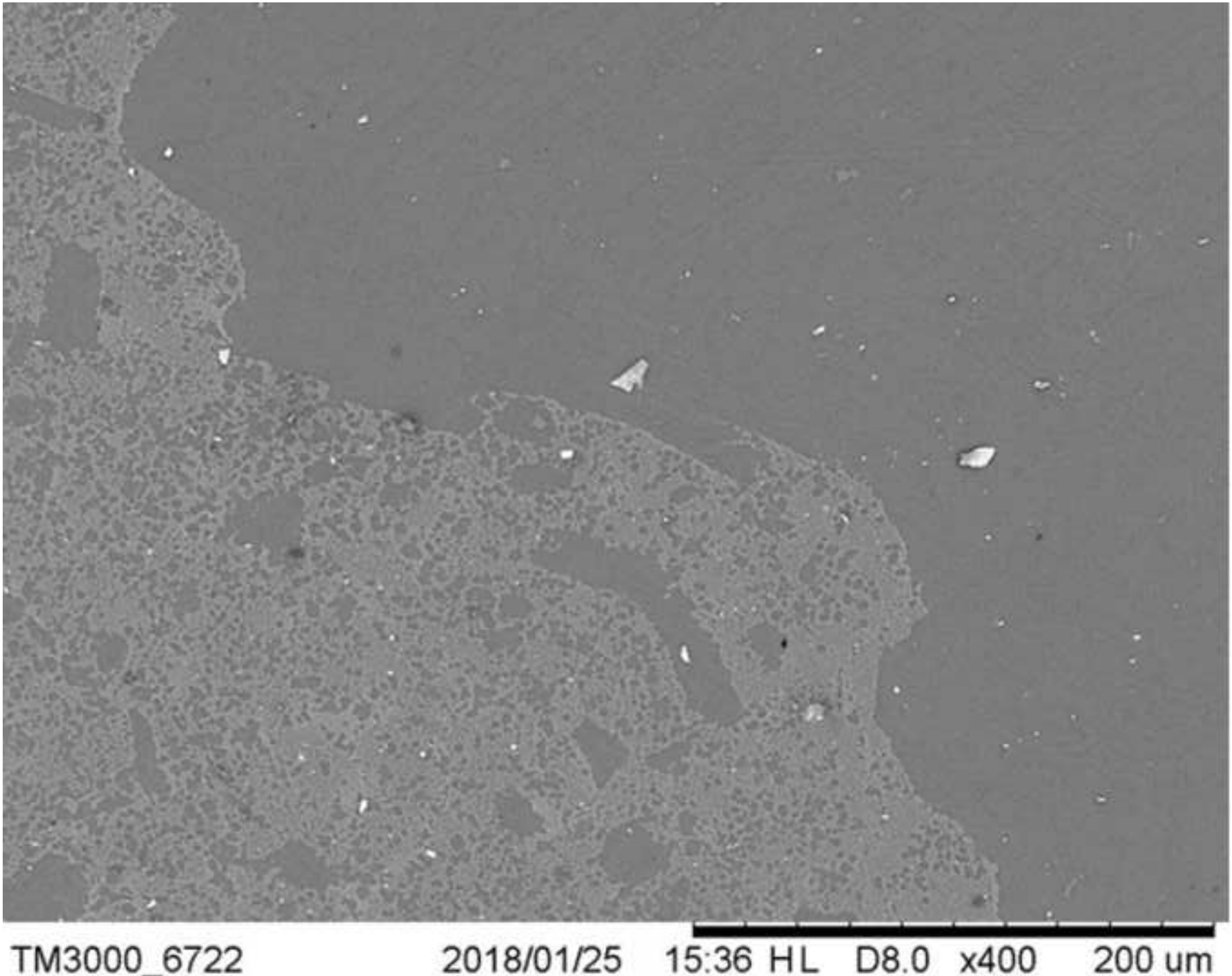

Figure 9
Click here to download high resolution image

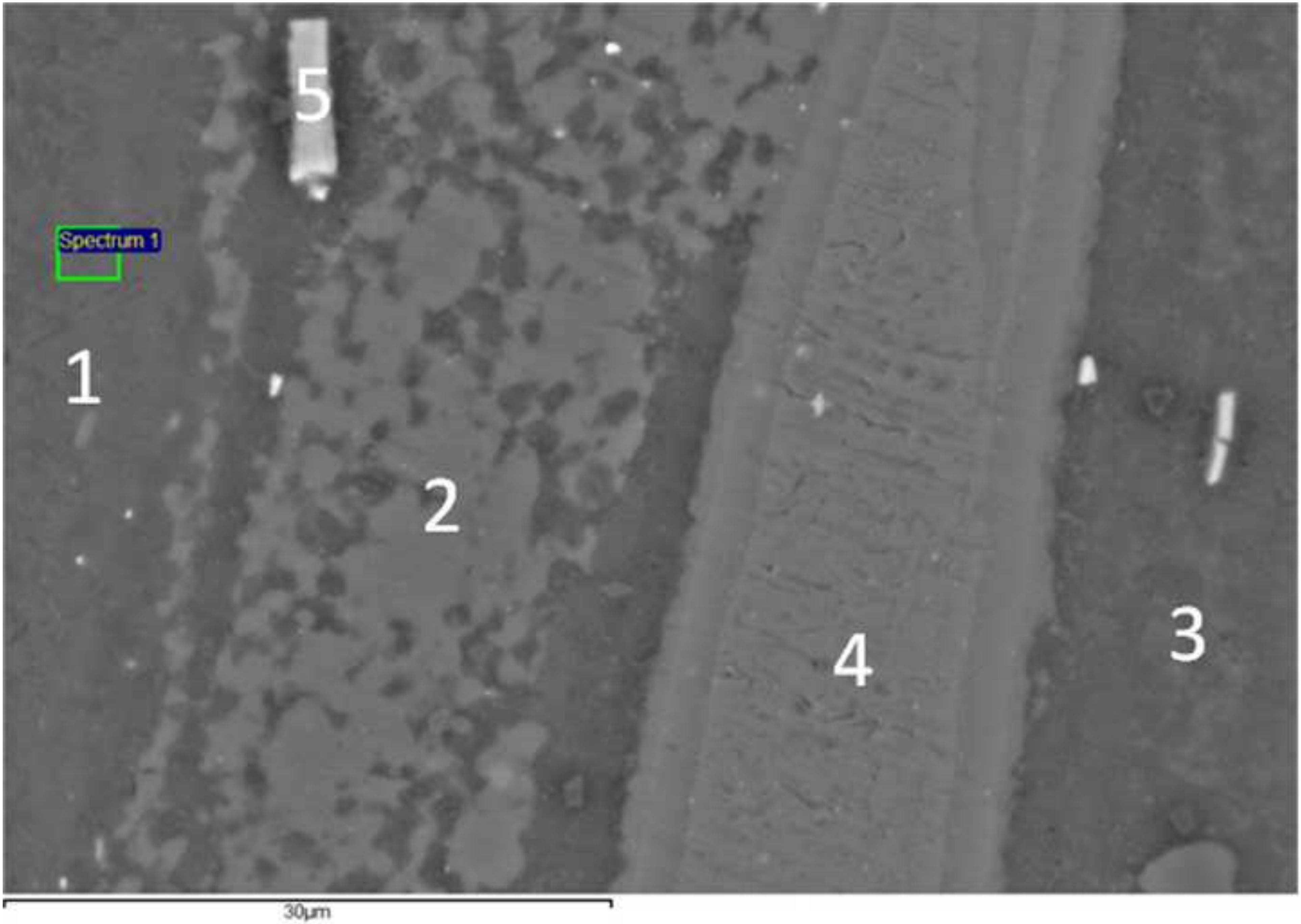

Figure 10

Click here to download high resolution image

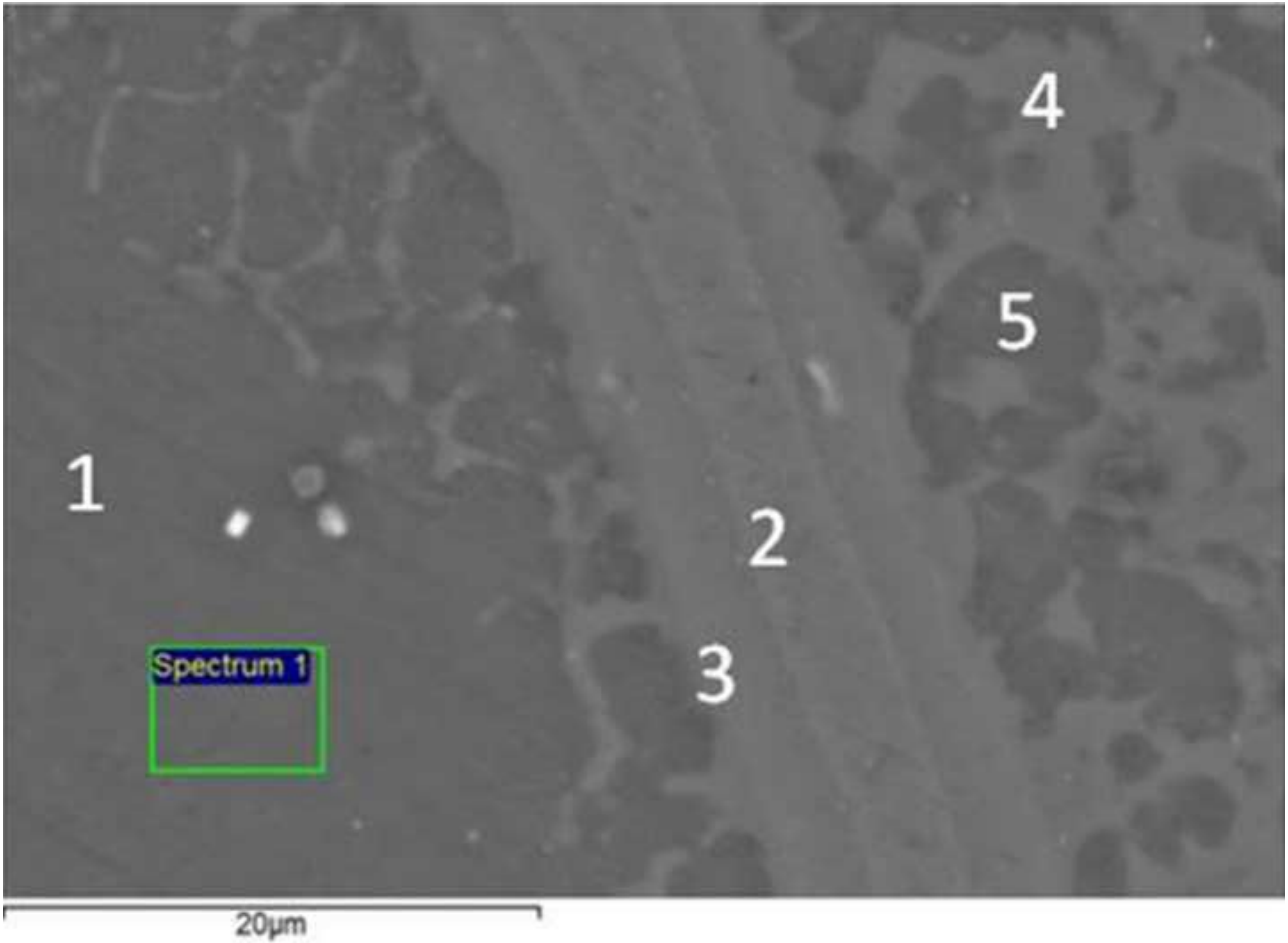

Figure 11
Click here to download high resolution image

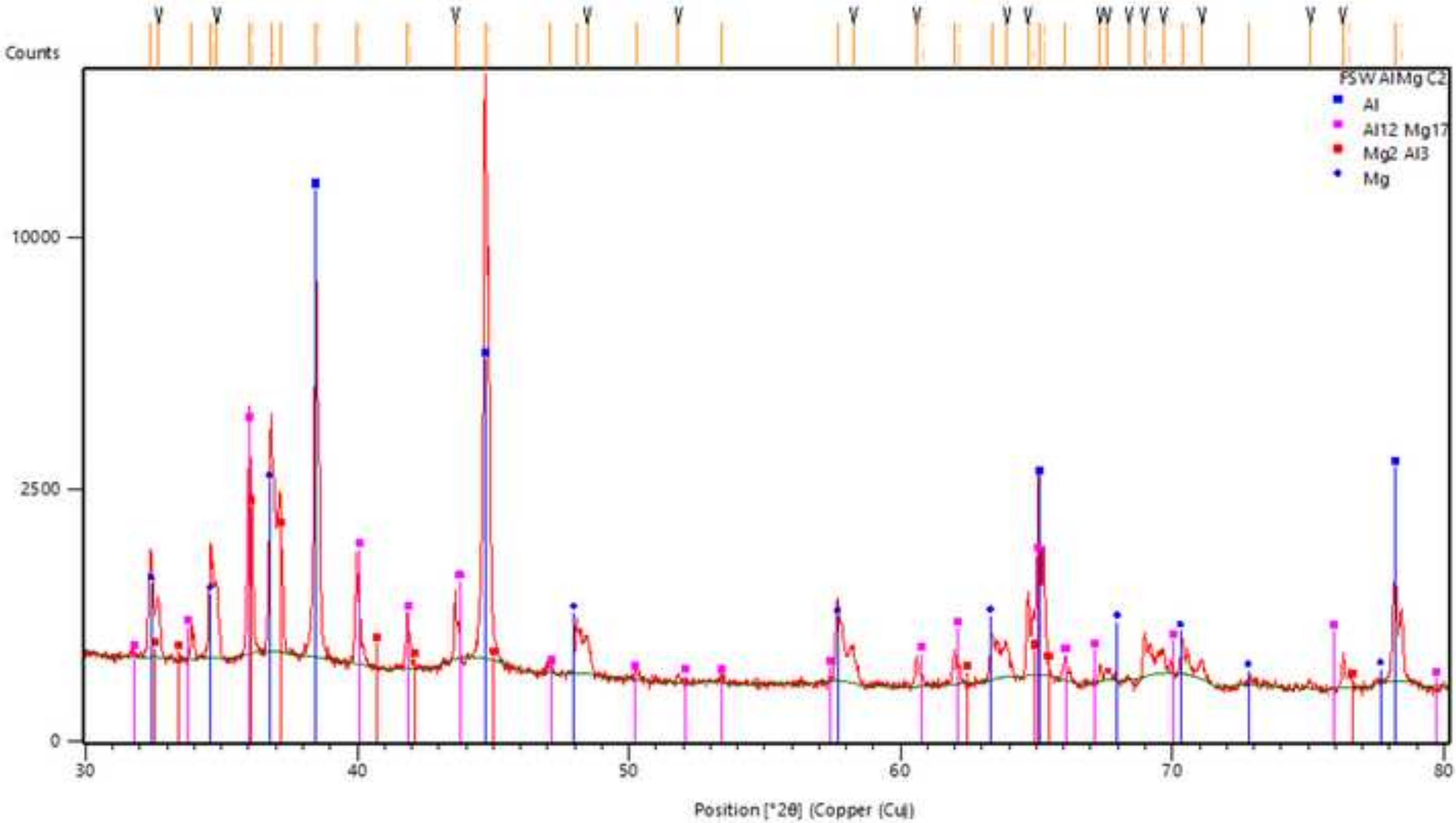

Figure 12
Click here to download high resolution image

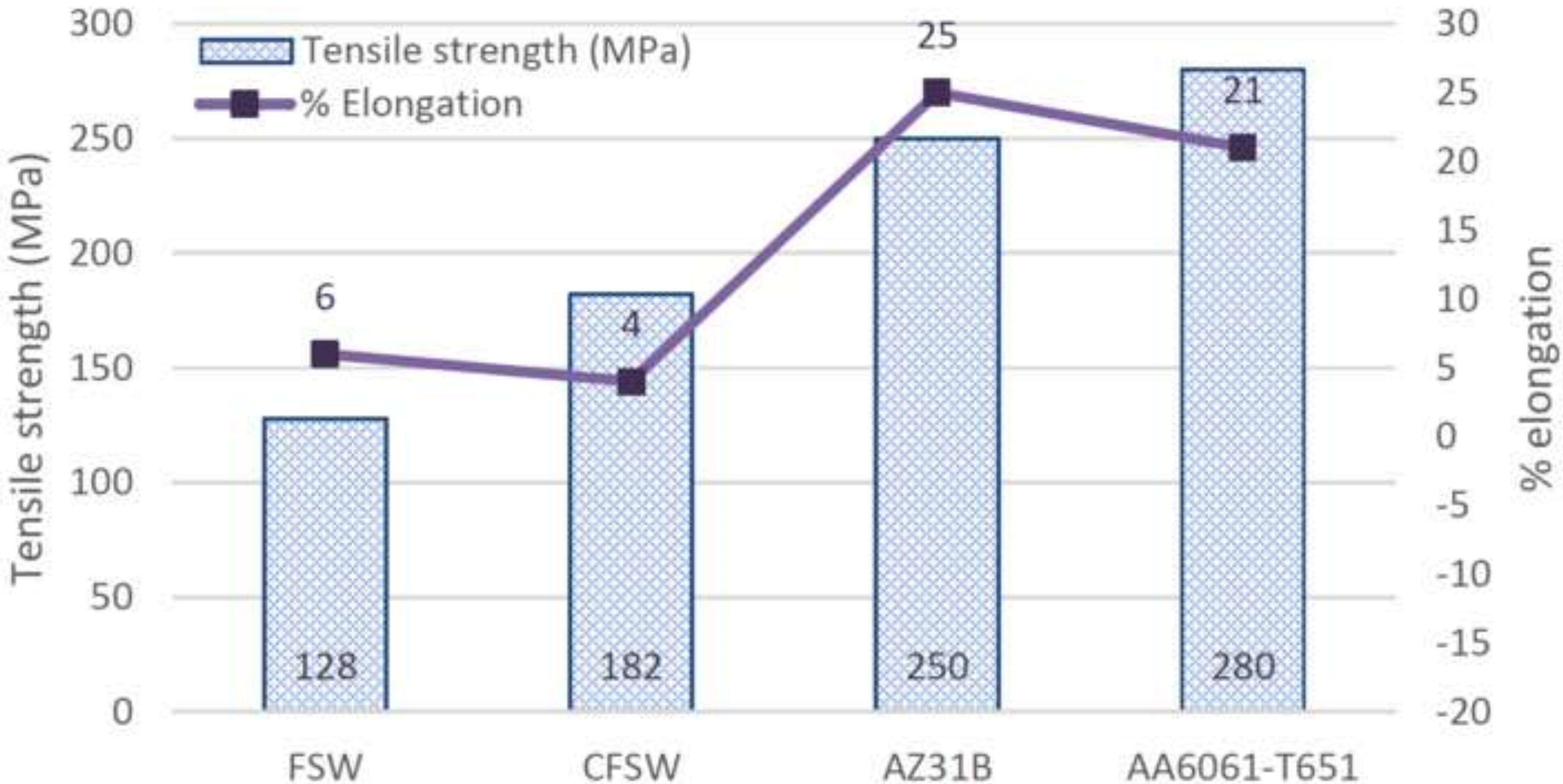

Figure 13

Click here to download high resolution image

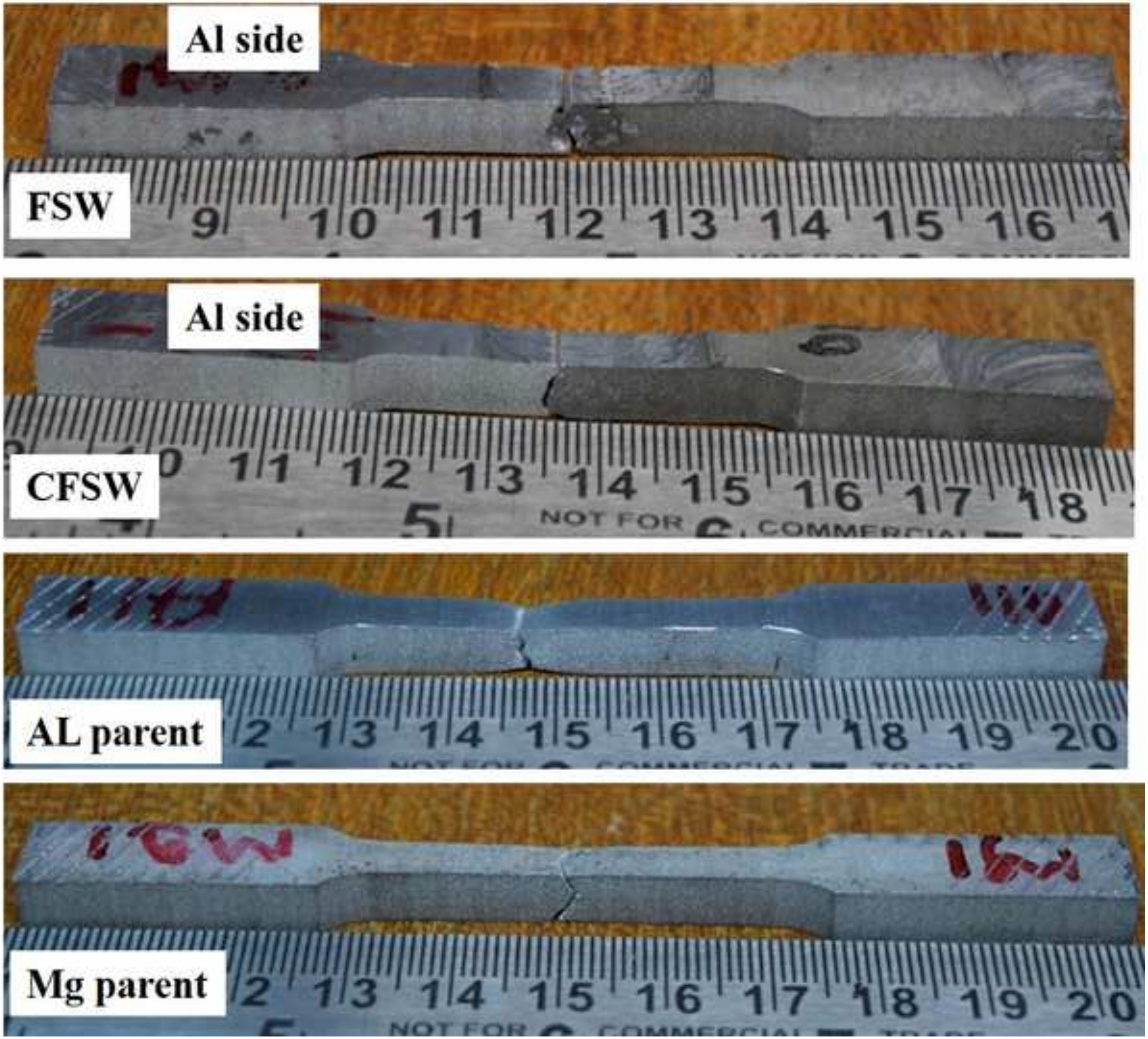

Figure 14
Click here to download high resolution image

Figure 15
Click here to download high resolution image

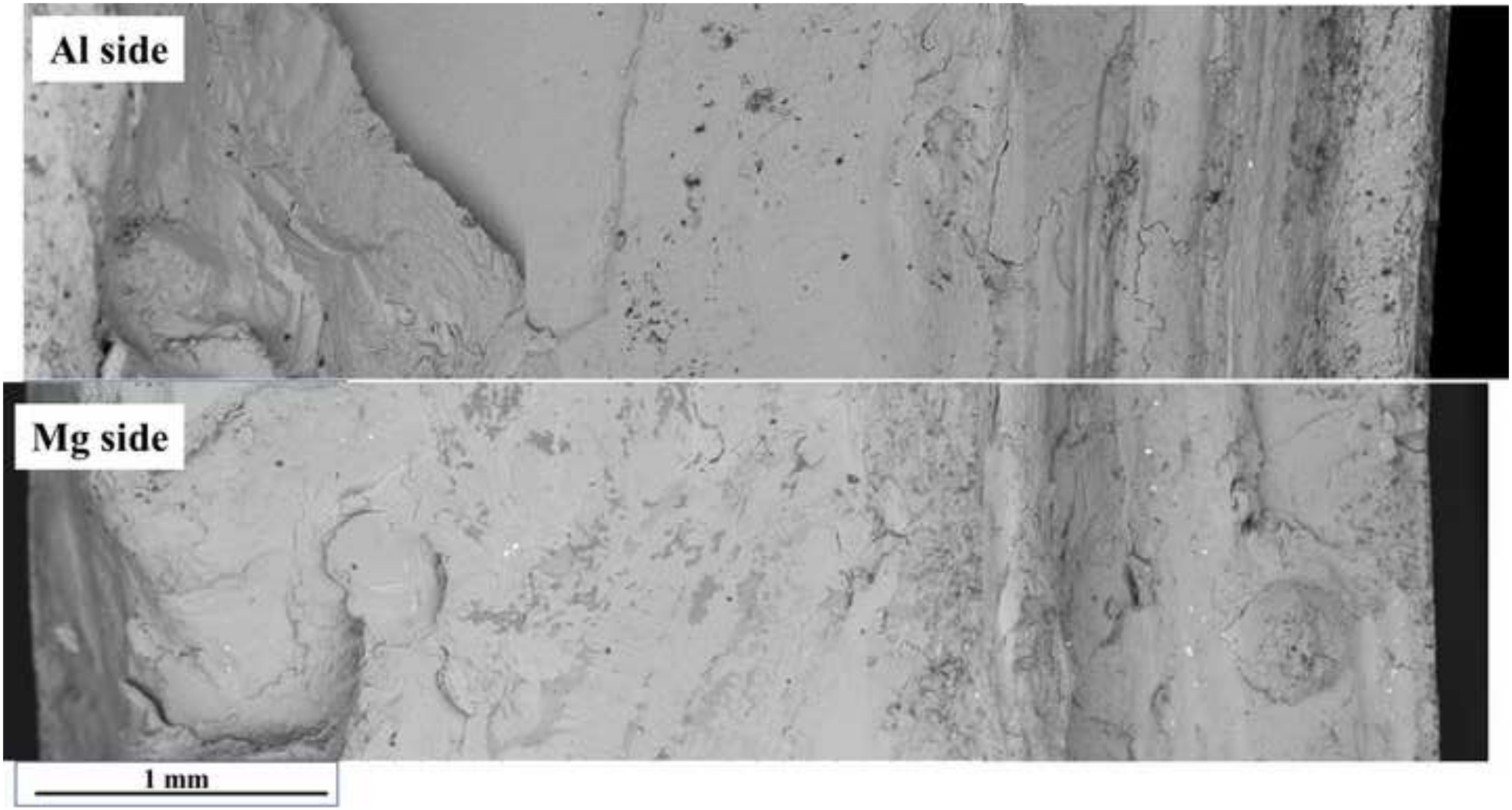

Figure 16

Click here to download high resolution image

Figure 17
Click here to download high resolution image

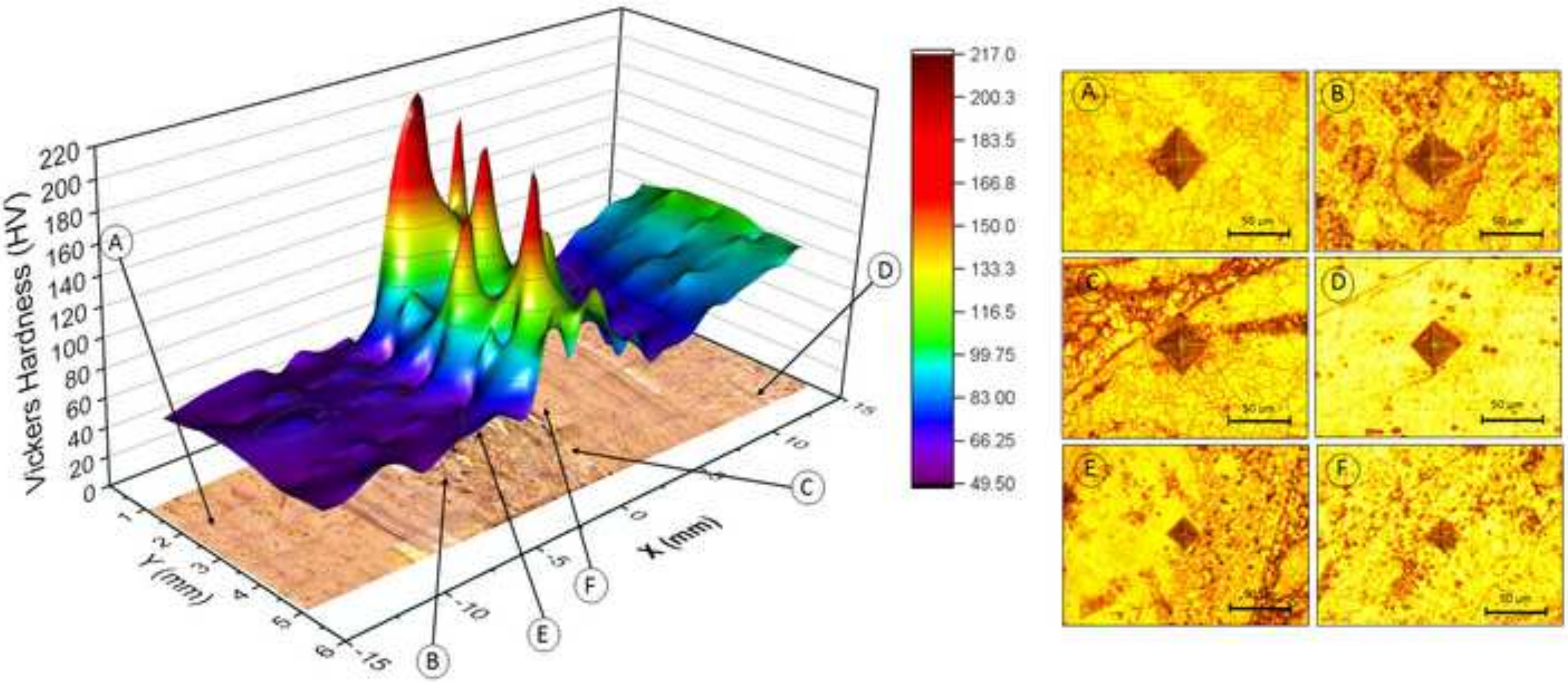

Figure 18
Click here to download high resolution image